Article

Cell Metabolism

Pharmacological Activation of Pyruvate Kinase M2 Inhibits CD4$^+$ T Cell Pathogenicity and Suppresses Autoimmunity

Graphical Abstract

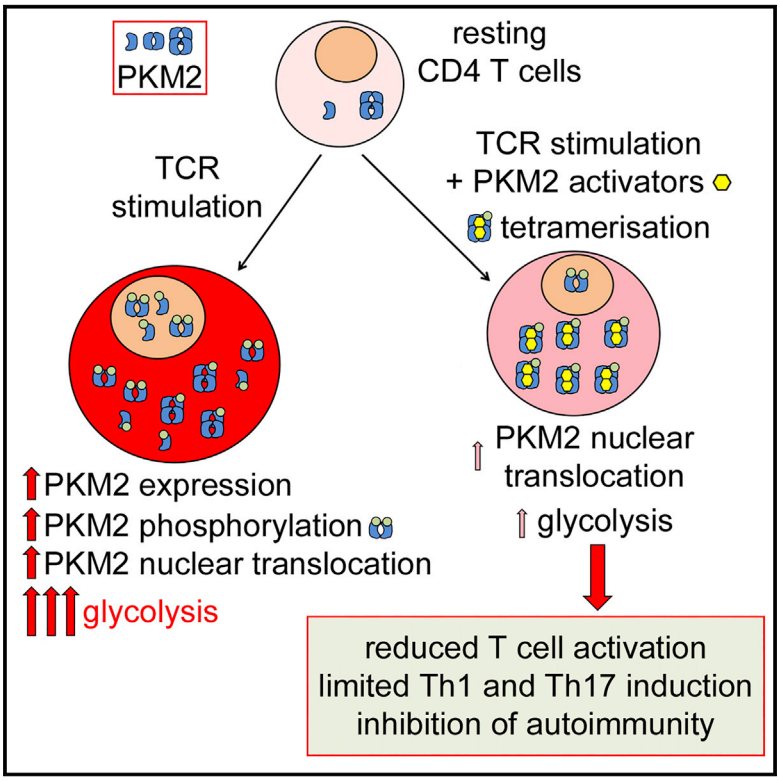

Highlights

- PKM2 translocates into the nucleus of CD4$^+$ T cells upon TCR stimulation
- TEPP-46 induces PKM2 tetramerization and blocks PKM2 nuclear translocation
- TEPP-46 limits T cell activation by inhibiting glycolysis in T cells
- TEPP-46 inhibits Th17 and Th1 polarization and EAE development *in vivo*

Authors

Stefano Angiari, Marah C. Runtsch, Caroline E. Sutton, ..., Erika L. Pearce, Kingston H.G. Mills, Luke A.J. O'Neill

Correspondence

angiaris@tcd.ie (S.A.),
laoneill@tcd.ie (L.A.J.O.)

In Brief

Angiari et al. show that the glycolytic enzyme PKM2 translocates into the nucleus of CD4$^+$ T cells upon TCR stimulation. PKM2 tetramerization by small-molecule PKM2 activators blocks its nuclear translocation and engagement of glycolysis, inhibiting T cell activation, Th17 and Th1 polarization, and development of EAE *in vivo*.

Angiari et al., 2020, Cell Metabolism *31*, 391–405
February 4, 2020
https://doi.org/10.1016/j.cmet.2019.10.015

CellPress

Cell Metabolism
Article

Pharmacological Activation of Pyruvate Kinase M2 Inhibits CD4+ T Cell Pathogenicity and Suppresses Autoimmunity

Stefano Angiari,[1,5,*] Marah C. Runtsch,[1,4] Caroline E. Sutton,[1,4] Eva M. Palsson-McDermott,[1] Beth Kelly,[2] Nisha Rana,[2] Harry Kane,[1] Gina Papadopoulou,[3] Erika L. Pearce,[2] Kingston H.G. Mills,[1] and Luke A.J. O'Neill[1,*]
[1]School of Biochemistry and Immunology, Trinity Biomedical Sciences Institute, Trinity College Dublin, 152–160 Pearse Street, Dublin D02 R590, Ireland
[2]Max Planck Institute of Immunobiology and Epigenetics, 79108 Freiburg, Germany
[3]Cellular Immunology Laboratory, Center for Basic Research, Biomedical Research Foundation of the Academy of Athens 115 27, Athens, Greece
[4]These authors contributed equally
[5]Lead Contact
*Correspondence: angiaris@tcd.ie (S.A.), laoneill@tcd.ie (L.A.J.O.)
https://doi.org/10.1016/j.cmet.2019.10.015

SUMMARY

Pyruvate kinase (PK) catalyzes the conversion of phosphoenolpyruvate to pyruvate during glycolysis. The PK isoform PKM2 has additional roles in regulation of gene transcription and protein phosphorylation. PKM2 has been shown to control macrophage metabolic remodeling in inflammation, but its role in T cell biology is poorly understood. Here, we report PKM2 upregulation, phosphorylation, and nuclear accumulation in murine and human CD4+ T cells following activation *in vitro*. Treatment of T cells with TEPP-46, an allosteric activator that induces PKM2 tetramerization and blocks its nuclear translocation, strongly reduces their activation, proliferation, and cytokine production by inhibiting essential signaling pathways and thus preventing the engagement of glycolysis. TEPP-46 limits the development of both T helper 17 (Th17) and Th1 cells *in vitro* and ameliorates experimental autoimmune encephalomyelitis (EAE) *in vivo*. Overall, our results suggest that pharmacological targeting of PKM2 may represent a valuable therapeutic approach in T cell-mediated inflammation and autoimmunity.

INTRODUCTION

Both innate and adaptive immune cells undergo substantial metabolic reprogramming following activation (Pearce and Pearce, 2013; O'Neill et al., 2016). In particular, complex regulation of the intracellular metabolic profile has been observed in T lymphocytes. It is now well established that naive T cells preferentially use oxidative phosphorylation (OXPHOS) and fatty acid oxidation (FAO) in their catabolic metabolism (Geltink et al., 2018). However, upon T cell receptor (TCR) ligation and costimulation, T cells engage aerobic glycolysis and Warburg metabolism, which are crucial for proper commitment of effector functions (Pearce and Pearce, 2013; O'Neill et al., 2016; Geltink et al., 2018). Of note, among CD4+ T cell subsets, sustained aerobic glycolysis was observed in activated effector T cells such as T helper 1 (Th1), Th2, and Th17 cells, whereas memory T cells present a naive-like metabolic profile, preferentially using OXPHOS and FAO for their energy supply. This suggests that specific metabolic profiles govern the phenotype of T cell subsets (Geltink et al., 2018). Importantly, previous studies indicate that interfering with intracellular metabolic pathways in immune cells represents a novel attractive therapeutic approach in inflammation (O'Neill et al., 2016; Freitag et al., 2016; Bettencourt and Powell, 2017).

The enzyme pyruvate kinase (PK) plays a crucial role in glycolysis, as it catalyzes the irreversible conversion of

Context and Significance

CD4+ T cells represent an immune cell population essential to remove pathogens from the organism and for long-term immunity, for example, after vaccination. However, over-activation of CD4+ T cells may be harmful for the body, causing development of immune-related pathologies such as autoimmune and allergic diseases. The protein pyruvate kinase (PK) is important for the function of certain types of immune cells, but its role in T cells is currently unknown. Researchers at the Trinity College in Dublin, Ireland, show that targeting PK activity, in particular of its isoform PKM2, limits excessive activation of CD4+ T cells and prevents the development of autoimmunity. The authors thus identify PKM2 as a potential therapeutic target for the treatment of inflammatory diseases caused by T cell over-activation.

phosphoenolpyruvate to pyruvate, that can in turn be used to fuel the tricarboxylic acid cycle (TCA) or converted to lactate, which is then secreted. In mammals, four different isoforms of PK were identified, but immune cells preferentially express the isoforms PKM1 and PKM2, which are generated by alternative splicing of the *PKM* gene (Israelsen and Vander Heiden, 2015; Palsson-McDermott et al., 2015). PKM1 is present in cells as a tetrameric protein that is highly active enzymatically and efficiently converts PEP to pyruvate and is usually expressed in terminally differentiated tissues, which require a large supply of ATP generated from pyruvate oxidation in the TCA cycle and OXPHOS (Israelsen and Vander Heiden, 2015; Dong et al., 2016). PKM2 is mainly present as a monomer/dimer in tissues with anabolic functions, including proliferating cells and cancer cells, and is subject to complex allosteric regulation that controls its enzymatic activity (Israelsen and Vander Heiden, 2015; Dong et al., 2016; Dayton et al., 2016). Monomeric/dimeric PKM2 is enzymatically less active than the tetrameric isoform, and its expression is essential in proliferating cells to divert glycolytic intermediates to pathways such as the pentose phosphate pathway (PPP) for nucleotide synthesis necessary for cell activation and proliferation (Lunt et al., 2015).

In recent years, so-called moonlighting activities of monomeric/dimeric PKM2 beyond its canonical enzymatic function have been discovered, such as regulation of gene expression and protein kinase activity (Israelsen and Vander Heiden, 2015; Dayton et al., 2016; Prakasam et al., 2018). In particular, monomeric/dimeric PKM2 was shown to translocate into the nucleus of cancer cells to stabilize the transcription factor hypoxia-inducible factor 1-alpha (HIF-1α) and to favor the expression of genes associated with glycolysis (Luo et al., 2011). Dimeric PKM2 has also been shown to play a critical role in inflammatory macrophage activation (Palsson-McDermott et al., 2015). The importance of PKM2 in T cell biology is however largely unknown. Previous work has shown that, upon TCR activation, T cells upregulate PKM2 expression (Wang et al., 2011; Cao et al., 2014). Furthermore, a role for PKM2 in T cell activation and function was suggested by a recent paper reporting that deletion of PKM2 in T cells inhibits production of interferon (IFN)-γ following activation with homocysteine (Lü et al., 2018). However, the possibility of controlling T cell activation and pathogenic potential upon TCR stimulation by modulating PKM2 activity pharmacologically has not been investigated thus far. In this study, we report that induction of tetrameric PKM2 with the small molecule activator TEPP-46 blocks the nuclear translocation of PKM2 and severely impacts T cell activation and pathogenicity both *in vitro* and *in vivo*. TEPP-46 limited Th17 and Th1 cell development *in vitro* and inhibited the development of experimental autoimmune encephalomyelitis (EAE). Our work suggests that pharmacological targeting of PKM2 may represent a valuable approach to control T cell-mediated inflammation and autoimmunity.

RESULTS

PKM2 Upregulation, Phosphorylation, and Nuclear Translocation in CD4$^+$ T Cells upon TCR Activation

To evaluate a potential role for PKM2 in T cell activation and functionality, we first analyzed PKM2 expression in murine CD4$^+$CD62L$^+$ T cells before and after CD3/CD28 stimulation *in vitro*. As previously reported (Wang et al., 2011; Cao et al., 2014), following TCR activation, we observed a time-dependent upregulation of PKM2 at both mRNA and protein levels (Figures 1A and 1B). Interestingly, isoform PKM1 mRNA and protein were also upregulated upon stimulation, but the expression levels of *Pkm2* were much higher in both resting and activated T cells, compared to *Pkm1*, being at least 30-fold higher (Figures S1A–S1C), indicating that T cells preferentially express PKM2 over PKM1. Of note, at all stages of activation, a significant proportion of PKM2 was found to be phosphorylated on tyrosine 105 (Y105), a modification that is known to limit the formation of the PKM2 tetrameric isoform (Figure 1C) (Prakasam et al., 2018; Hitosugi et al., 2009). Accordingly, we observed an increase in both the monomeric/dimeric and the tetrameric forms of PKM2 upon T cell activation (Figure 1D). PKM2 upregulation was also paralleled by its time-dependent phosphorylation on serine 37 (S37) (Figure 1E), a modification that was reported to facilitate its translocation into the nucleus (Prakasam et al., 2018; Yang et al., 2012a). In accordance, CD3/CD28 stimulation led to the time-dependent accumulation of PKM2 in the nucleus, with a concomitant upregulation of PKM2 expression also in the cytoplasm (Figure 1F). Overall, these data indicate a potential role for PKM2 moonlighting functions in T cell activation.

Induction of PKM2 Tetramerization Blocks Murine CD4$^+$ T Cell Activation

Given the induction of monomeric/dimeric PKM2 and its nuclear localization in activated CD4$^+$ T cells, we sought to determine the effect of the PKM2 modulator TEPP-46 on T cell function. TEPP-46 is a well-characterized allosteric activator of PKM2 that causes its tetramerization, blocks its translocation into the nucleus, and increases its canonical enzymatic activity (Palsson-McDermott et al., 2015; Anastasiou et al., 2012). To test its impact on T cell function, we treated resting CD4$^+$CD62L$^+$ T cells with TEPP-46 at 50 and 100 μM, doses that were shown to limit PKM2-mediated activation of inflammatory macrophages *in vitro* (Palsson-McDermott et al., 2015). We initially confirmed that treatment of murine CD4$^+$CD62L$^+$ T cells with TEPP-46 during CD3/CD28 activation-induced PKM2 tetramerization, which was increased at 50 μM and especially at 100 μM (Figure S2A). Notably, TEPP-46 also reduced the nuclear levels of PKM2 in activated T cells, in a dose-dependent manner (Figure S2B), and had no cytotoxic effect on T cells at both the concentrations used (Figure S2C). We then investigated the effect of TEPP-46 treatment on T cell functionality. We first observed a dramatic reduction in the early levels of interleukin-2 (IL-2) mRNA in TEPP-46-treated cells, compared to control (CTRL) cells, 24 h after CD3/CD28 stimulation (Figure 2A). In accordance, TEPP-46-treated T cells produced much less IL-2 following restimulation *in vitro*, suggesting a defect in early T cell activation associated with TEPP-46 treatment (Figure 2B). We next found that TEPP-46 inhibited the proliferation of murine CD4$^+$ T cell in a dose-dependent manner (Figure 2C). TEPP-46 also significantly blocked T cell activation, as evident by increased CD62L and reduced CD44 and CD25 expression in CD4$^+$ T cells treated with TEPP-46, compared to control

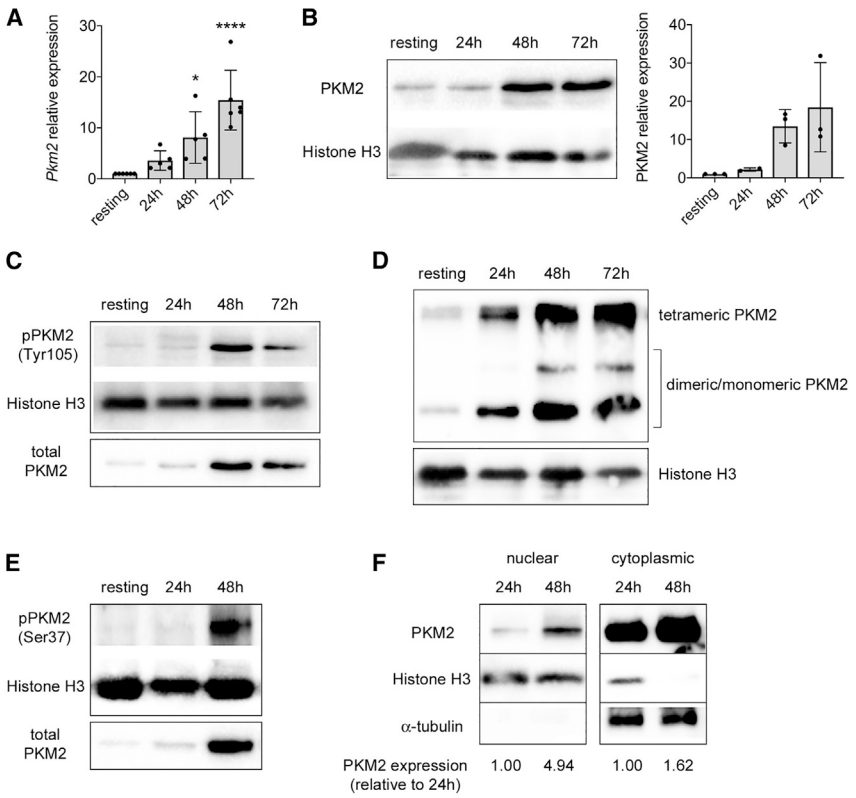

Figure 1. CD3/CD28 Activation Induces PKM2 Expression and Nuclear Accumulation in Murine CD4$^+$CD62L$^+$ T Cells

Murine CD4$^+$CD62$^+$ T cells were stimulated *in vitro* for 3 days with CD3/CD28 antibodies and collected at different time points of activation.

(A) Quantification of *Pkm2* mRNA in resting versus activated murine CD4$^+$CD62L$^+$ T cells by qRT-PCR (n = 5–6 from 4 independent experiments). *p < 0.05 and ****p < 0.0001 compared to resting condition, by one-way ANOVA with Dunnett's post-hoc test.

(B) Left, western blot showing upregulation of PKM2 protein in CD4$^+$CD62L$^+$ T cells following activation. Right, quantification of PKM2 expression by densitometry analysis (n = 2–3 mice from 2 independent experiments).

For (A and B), data are the mean ± standard deviation (SD).

(C) Western blots showing time-dependent increase in PKM2 phosphorylation on tyrosine 105 (Tyr105) in activated murine CD4$^+$ T cells. One representative experiment out of two is shown.

(D) Cells were collected at different time points of activation, crosslinked with DSS, and analyzed for PKM2 expression. A representative western blot displaying upregulation of monomeric/dimeric and tetrameric PKM2 in activated T cells is shown.

(E) Western blots showing time-dependent increase in PKM2 phosphorylation on serine 37 (Ser37) in activated murine CD4$^+$ T cells.

(F) Cells were collected at different time points of activation. Nuclear and cytoplasmic fractions were isolated by cell fractionation and analyzed for PKM2 expression by western blot. A representative blot showing accumulation of PKM2 in the nucleus and its upregulation in the cytoplasm of activated murine CD4$^+$CD62L$^+$ T cells is presented.

For (D), (E), and (F), one representative experiment out of two-three is shown.

treatment (Figure 2D). Consistent with these results, induction of PKM2 tetramerization inhibited the expression of tumor necrosis factor-alpha (TNF-α) mRNA by T cells, which indeed produced less TNF-α protein upon restimulation *in vitro* (Figures 2E and 2F). Importantly, we also observed reduced T cell proliferation, activation, and IL-2 production upon treatment with DASA-58, another well-characterized PKM2 allosteric activator (Figures S3A–S3C) (Anastasiou et al., 2012). Strikingly, TEPP-46 treatment also enhanced the expression of forkhead box P3 (Foxp3) mRNA in activated unpolarized T cells (Figure S4A). This was associated with a small but significant increase in the percentage of Foxp3$^+$CD25$^+$ cells induced by TEPP-46 (Figure S4B). Importantly, we also observed TEPP-46-dependent induction of Foxp3$^+$CD25$^+$ cells from CD3/CD28-activated naive CD25$^-$ T cells, which are depleted of the naturally occurring regulatory T cell (Treg) population (Figures S4C and S4D). Surprisingly, despite inducing Tregs under non-polarizing conditions, TEPP-46 inhibited the generation of Tregs induced by TGF-β *in vitro*, by blocking the phosphorylation of signal transducer and activator of transcription 5 (Stat5) induced by TGF-β (Figures S4E and S4F). These results suggest that, by inducing PKM2 tetramerization and blocking its nuclear translocation, TEPP-46 inhibits T cell activation and may favor the generation of Tregs under non-polarizing conditions.

TEPP-46 Reduces Myc, HIF-1α, and mTORC1 Signaling and Engagement of Glycolysis in T Cells

To evaluate the overall impact of TEPP-46 treatment on the activation and functionality of CD4$^+$ T cells, we performed global gene expression analysis by RNA sequencing (RNA-seq), comparing TEPP-46-treated T cells to activated CTRL cells and resting T cells. We first observed that treatment with TEPP-46 was associated with a global change in gene expression in T cells, compared to CTRL cells (Figures S5A and S5B). Unbiased analysis confirmed the modulation of T cell activation by TEPP-46, with TEPP-46-treated cells showing an expression profile similar to that of resting cells (Figure S5C). Importantly, TEPP-46 treatment did not induce skewing of T cells to a specific T cell subset and did not favor the development of memory T cells (data not shown). Our data also indicated that TEPP-46 did not induce a global regulatory phenotype in T cells, suggesting that the induction of Foxp3$^+$CD25$^+$ cells observed in the presence of TEPP-46 might not lead to the generation of functional Treg cells (Figure S5D). Notably, unbiased pathway analysis predicted downregulation of key signaling pathways involved in T cell activation by TEPP-46, among which were the Myc, HIF-1α, and the mammalian target of rapamycin (mTOR) pathways (Figure 3A). In accordance, gene expression analysis confirmed that TEPP-46 treatment severely impaired the upregulation of Myc-, HIF-1α-, and

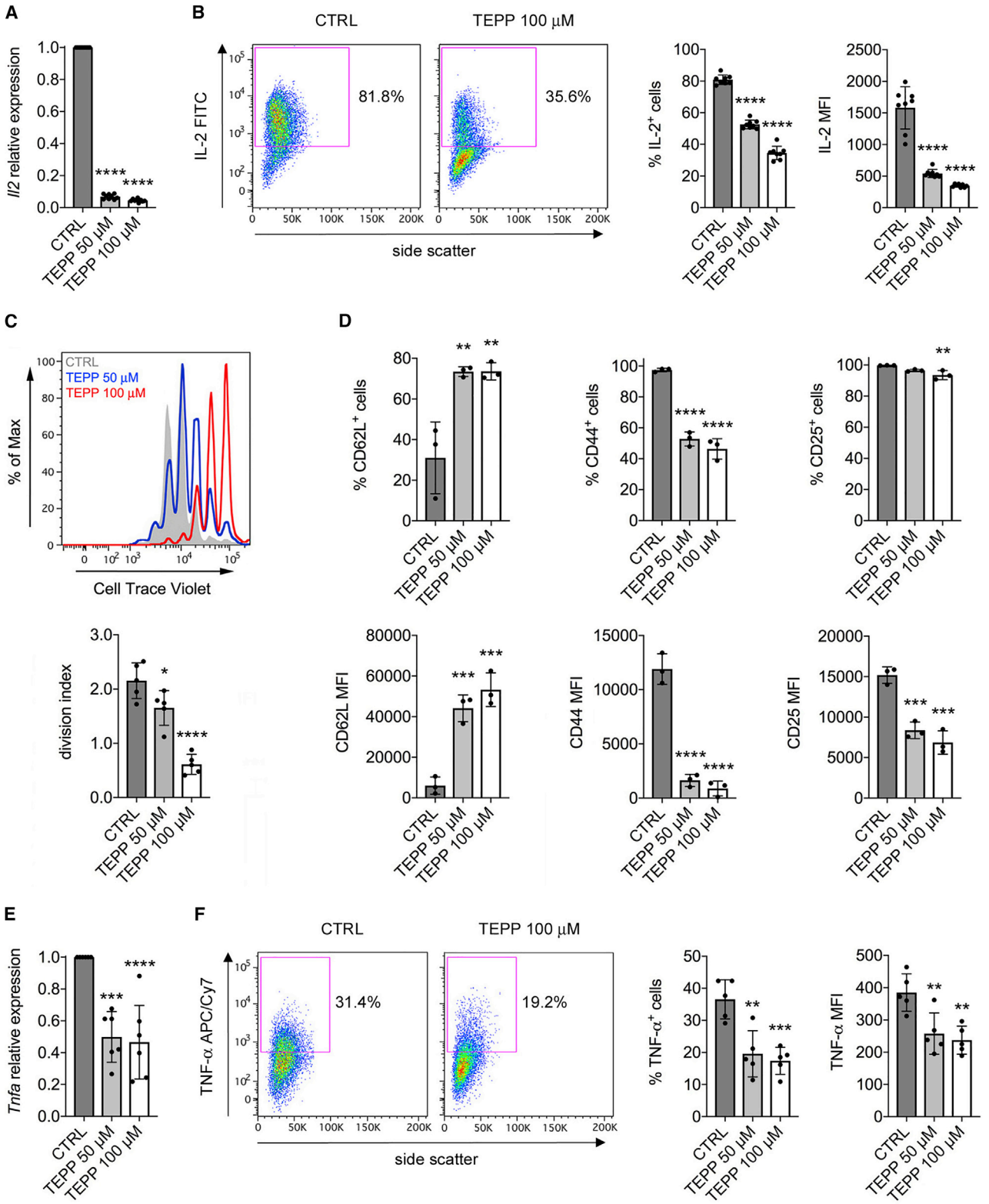

Figure 2. PKM2 Tetramerization Blocks T Cell Activation *In Vitro*

Murine CD4$^+$CD62$^+$ T cells were stimulated *in vitro* with CD3/CD28 antibodies in the presence of DMSO (CTRL), TEPP-46 50 μM, or 100 μM.

(A and B) Cells were collected after 24 h of stimulation.

(A) Quantification of *Il2* mRNA in activated T cells by qRT-PCR (n = 9 from three independent experiments).

(legend continued on next page)

mTOR-induced genes in $CD4^+$ T cells upon activation *in vitro* (Figure 3B).

As Myc, HIF-1α, and mTOR are essential players in T cell activation and functionality (Geltink et al., 2018), we focused on these pathways, and we confirmed their inhibition in TEPP-46-treated T cells. We first checked for early Myc protein and mRNA expression 24 h after CD3/CD28 stimulation, and we observed a reduction in both Myc protein and mRNA levels following TEPP-46 treatment (Figures S6A and S6B). We then evaluated the functionality of mTOR, in particular the mTORC1 complex, in TEPP-46-treated cells, analyzing the phosphorylation of p70 S6 and p85 S6 kinases, a well-established readout of mTORC1 activity. We found that TEPP-46 treatment led to a strong reduction in the phosphorylation of these proteins 24 h after activation *in vitro*, suggesting that PKM2 tetramerization might block mTORC1 activity in T cells (Figure S6C). We then observed that TEPP-46-treated murine $CD4^+$ T cells displayed a strongly reduced HIF-1α expression after 3 days of *in vitro* activation, compared to control cells (Figure S6D). Importantly, TEPP-46 did not affect the levels of *Hif1a* mRNA (Figure S6E), supporting a role for nuclear PKM2 in HIF-1α stabilization rather than transcription (Luo et al., 2011).

HIF-1α, Myc, and mTORC1 are key regulators of aerobic glycolysis and Warburg-like metabolism in T cells (Geltink et al., 2018). We thus speculated that TEPP-46 might modulate T cell activation by limiting the engagement of glycolysis. We, therefore, analyzed the effect of TEPP-46 on the glycolytic potential of T cells. First, analysis of RNA-seq data and qRT-PCR experiments indicated that TEPP-46 treatment significantly blocked the induction of several glycolytic genes in T cells upon activation, including the glucose transporter *Slc2a1* (Glut-1), which controls glucose uptake upon TCR activation and is essential for engagement of aerobic glycolysis in T cells (Figures 3C and S6F) (Geltink et al., 2018; Macintyre et al., 2014). Second, by performing Seahorse analysis, we confirmed that TEPP-46 treatment severely impaired glycolysis in T cells, in terms of both glycolytic rate and glycolytic capacity, while oxygen consumption rate (OCR) in TEPP-46-treated cells was similar to that of CTRL cells, confirming that TEPP-46 treatment specifically affects glycolysis engagement in T cells (Figures 3D and 3E). Overall, these results indicate that induction of PKM2 tetramerization blocks essential signaling pathways necessary for the engagement of aerobic glycolysis, a crucial step for T cell activation and effector functions.

PKM2 Tetramerization Constrains Th17 and Th1 Cell Development

HIF-1α, Myc, and mTORC1 activity and engagement of aerobic glycolysis are necessary for the generation of pro-inflammatory T cell subsets such as Th17 and Th1 cells (Geltink et al., 2018). Therefore, we next evaluated the impact of TEPP-46 treatment on the development of such T cell populations. For this purpose, we polarized resting murine $CD4^+CD62L^+$ T cells to Th17 or Th1 phenotypes in the presence of increasing concentrations of TEPP-46. We first confirmed that, as in unpolarized T cells, both Th17 and Th1 cells had increased PKM2 expression upon *in vitro* activation (Figures S7A and S7B). We next observed that TEPP-46 severely inhibited the generation of Th17 cells in a dose-dependent manner, as revealed by the strongly reduced percentage of IL-17A-producing cells upon TEPP-46 treatment (Figure 4A). In accordance with results obtained in unpolarized cells (Figure 2), TEPP-46 also limited the production of TNF-α by Th17 cells (Figure 4A). The block of Th17 induction was also confirmed at the mRNA level, with TEPP-46 reducing the expression of *Tnfa* and Th17 subset-specific cytokines *Il17a, Il17f, Il21*, whereas *Il22* was not modulated by the treatment (Figure 4B). Similar results were observed with DASA-58, which blocked Th17 cells development compared to CTRL treatment (Figure S3D). Strikingly, rather than inducing a global downregulation of transcription factors controlling Th17 development, TEPP-46 selectively impacted the expression levels of RAR-related orphan receptor alpha (Rorα; *Rora* gene), Interferon regulatory factor 4 (*Irf4*), and Runt-related transcription factor 1 (*Runx1*) (Figure 4C). mRNA levels of other transcription factors important for Th17 polarization such as RORγt (*Rorc* gene), aryl hydrocarbon receptor (*Ahr*), NF-kappa-B inhibitor zeta (*Nfkbiz*), and basic leucine zipper transcription factor, ATF-like (*Batf*) were not affected by the treatment (Figure 4C). Notably, PKM2 tetramerization led to a significant induction of *Foxp3* mRNA and $Foxp3^+CD25^+$ T cells in Th17-polarizing conditions (Figures S7C and S7D), confirming the data obtained with unpolarized cells (Figure S4).

We next analyzed the impact of PKM2 tetramerization on Th1 development. As with Th17 cells, TEPP-46 treatment strongly inhibited the generation of Th1 cells *in vitro*, reducing the production of IFN-γ and TNF-α at both protein and mRNA levels (Figures 5A and 5B). Similar to Th17 cells, DASA-58 also limited Th1 cell development *in vitro* (Figure S3E). Somewhat surprisingly, TEPP-46 did not affect the expression of T-box transcription factor TBX21 (T-bet; *Tbx21* gene), but strongly reduced the mRNA levels of Eomesodermin (*Eomes*), a key

(B) Cells were re-stimulated *in vitro* with PMA and ionomycin in the presence of brefeldin A. IL-2 production was then evaluated by flow cytometry after intracellular cytokine staining. Left, representative plot showing reduced IL-2 production by TEPP-46-treated cells. Right, quantification of the percentage of IL-2-producing cells and IL-2 mean fluorescence intensity (MFI) in CTRL versus TEPP-46-treated cells (n = 8 from 3 independent experiments).

(C–F) Cells were collected after 3 days of stimulation.

(C) Top, representative flow cytometry plot displaying T cell proliferation assessed as CellTrace violet dilution. Bottom, a division index was calculated with FlowJo software to quantify T cell proliferation (n = 5 from four independent experiments).

(D) Expression of surface CD62L, CD44, and CD25 was evaluated by flow cytometry. The percentage of expressing cells and the MFI are shown (n = 3 from 2 independent experiments).

(E) Quantification of *Tnfa* mRNA levels in activated T cells by qRT-PCR (n = 6 from 6 independent experiments).

(F) Cells were re-stimulated *in vitro* with PMA and ionomycin in the presence of brefeldin A. TNF-α production was then evaluated by flow cytometry after intracellular cytokine staining. Left, representative plot showing reduced TNF-α production by TEPP-46 treated cells. Right, quantification of the percentage of TNF-α-producing cells and TNF-α MFI in CTRL versus TEPP-46-treated cells (n = 5 from 2 independent experiments). For all panels, data are the mean ± SD. *p < 0.05, **p < 0.01, ***p < 0.001, or ****p < 0.0001 compared to CTRL condition, by one-way ANOVA with Dunnett's post-hoc test.

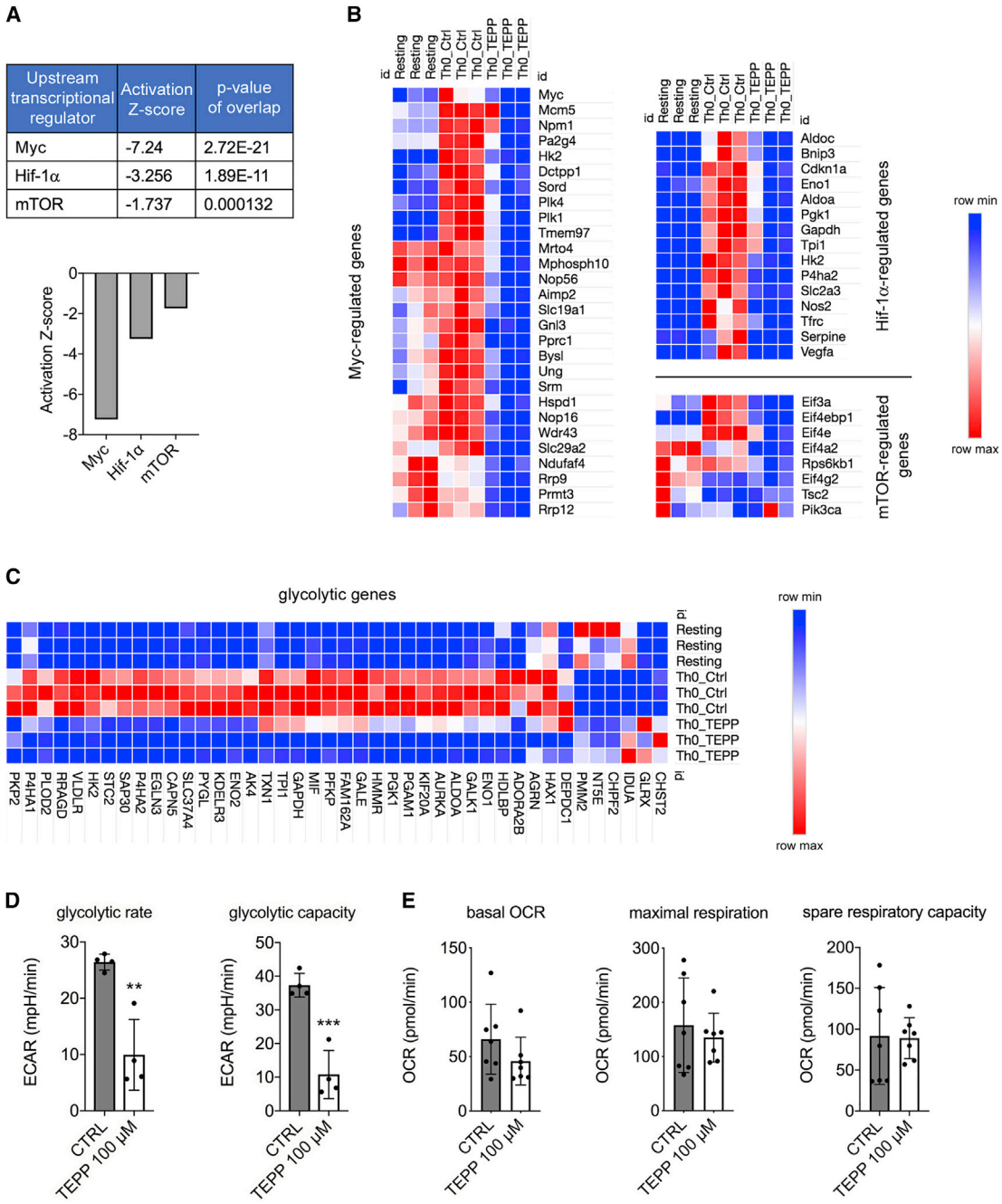

Figure 3. PKM2 Tetramerization Limits HIF1-α, Myc, and mTORC1 Signaling and Engagement of Glycolysis in CD4⁺ T Cells

Murine CD4⁺ T cells were collected after 72 h of *in vitro* activation with CD3/CD28 antibodies in the presence of DMSO (CTRL condition) or TEPP-46 100 μM.

(A) Results of unbiased Ingenuity Pathway Analysis predicting downregulation of Myc-, Hif-1-α-, and mTOR-regulated pathways by TEPP-46.

(B) Heatmaps showing expression of Myc-, Hif-1-α-, and mTOR-regulated genes in resting T cells and T cells activated in the presence of DMSO (Th0 Ctrl) or TEPP-46 (Th0 TEPP).

(C) Heatmap showing expression of glycolytic genes in resting, Th0 Ctrl, and Th0 TEPP-46 cells.

(D and E) Cells were tested for their glycolytic capacity and oxygen consumption rate (OCR) on a Seahorse XFe96 Analyzer.

(D) Quantitative analysis of glycolytic rate and glycolytic capacity of CTRL and TEPP-46-treated cells (n = 4 from 2 independent experiments).

(E) Quantitative analysis of basal OCR, maximum respiration and spare respiratory capacity of CTRL and TEPP-46-treated cells (n = 7 from three independent experiments). For (D) and (E), data are the mean ± SD. **p < 0.01 or ***p < 0.001, compared to CTRL condition, by two-tailed unpaired Student's t test.

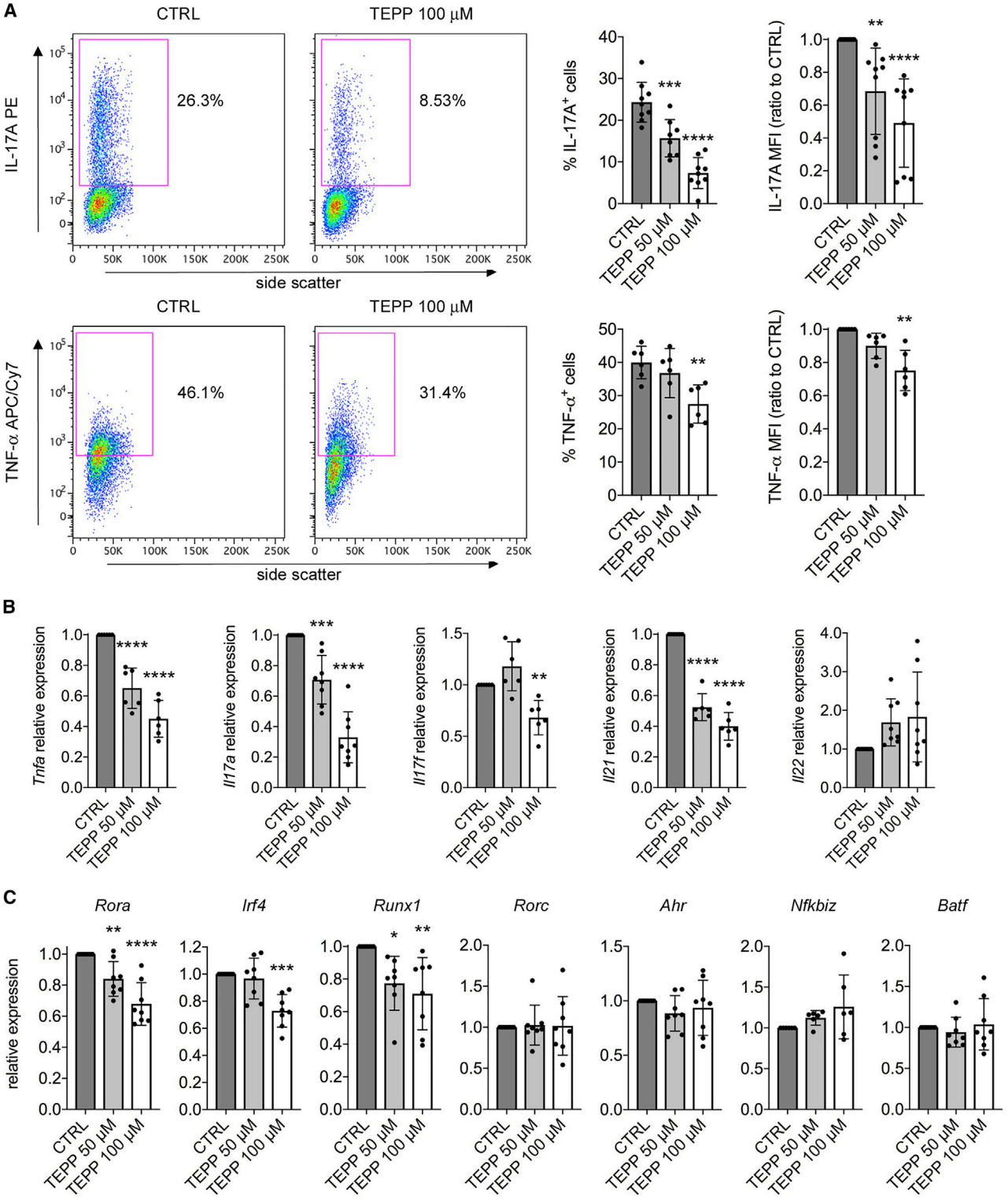

Figure 4. TEPP-46 Limits Th17 Cell Polarization

Murine $CD4^+CD62^+$ T cells were activated *in vitro* for 3 days with CD3/CD28 antibodies under Th17-polarizing conditions in the presence of DMSO (CTRL condition), TEPP-46 50 μM, or 100 μM.

(legend continued on next page)

transcription factor controlling Th1 cell development (Figure 5C) (Yang et al., 2008). Finally, as in unpolarized and Th17 cells, TEPP-46 treatment induced *Foxp3* expression and the generation of Foxp3$^+$CD25$^+$ cells also in Th1-polarized cells (Figures S7E and S7F). Overall, these results indicate that PKM2 modulates Th17/Th1 development by controlling the activity of specific transcription factors and demonstrate the potential of PKM2 tetramerization in inducing Treg cells under pro-inflammatory conditions.

TEPP-46 Inhibits the Development of EAE

Given the ability of PKM2 tetramerization to inhibit Th17/Th1 induction with a possible concurrent induction of Tregs *in vitro*, we tested the therapeutic potential of TEPP-46 in the autoimmune model EAE, in which Th1/Th17-mediated responses are essential for the induction of neuroinflammation (Kipp et al., 2017). We treated EAE mice every other day from day 0 to day +14 post-immunization with 50 mg/kg of TEPP-46 and evaluated disease development. We found that TEPP-46 markedly inhibited the development of EAE, with a significant reduction of the mean clinical score and prevention of weight loss, when compared to vehicle treatment (Figure 6A). This was accompanied by a substantial delay in the day of onset associated with TEPP-46 treatment (Figure 6B). Extending the treatment with TEPP-46 until day +20 post-immunization maintained the protective effect, but the results were not significant, as CTRL mice eventually recovered (data not shown). We then analyze the cellular infiltrates in the central nervous system (CNS; brain and spinal cord) of EAE mice. We first observed a significant reduction in the number of CD45$^+$ cells in the CNS of TEPP-46-treated mice, compared to vehicle-injected mice, suggesting a reduced leukocyte trafficking to the CNS associated with TEPP-46-treatment (Figure 6C). Strikingly, we observed no increase in the percentage of Foxp3$^+$CD25$^+$ T cells in the CNS of TEPP-46-treated animals (Figure 6D), suggesting that *in vivo* induction of Tregs is unlikely to be the mechanism of EAE inhibition by TEPP-46. However, the percentage of both CD4$^+$IL-17A$^+$ and CD4$^+$IFN-γ^+ cells was reduced in the CNS of TEPP-46-treated mice (Figure 6E). Of note, TEPP-46 treatment also reduced the percentage of granulocyte-macrophage colony-stimulating factor (GM-CSF)-producing CD4$^+$ T cells, which are crucial for the development of EAE (Kostic et al., 2018), as well as Ki67$^+$ cells, indicating a lower number of pathogenic and actively proliferating CD4$^+$ T cells in the CNS of TEPP-46-treated mice (Figure 6E). Of note, TEPP-46-treated mice also displayed a reduction in CD8$^+$ cells producing IFN-γ, IL-17A, and GM-CSF in the CNS, suggesting that PKM2 tetramerization may also block CD8$^+$ T cell pathogenic potential (Figure 6E). Overall, our data indicate a global anti-inflammatory effect of TEPP-46 in EAE and confirm the potential of PKM2 tetramerization as a novel therapeutic approach for the treatment of Th17/Th1-mediated pathologies.

To confirm that the effect of TEPP-46 *in vivo* is due to a direct block of T cell pathogenicity, we induced passive-transfer EAE in C56Bl/6 mice. We isolated CD3$^+$ T cells from myelin oligodendrocyte glycoprotein (MOG)$_{35–55}$-immunized mice, treated them with DMSO (CTRL cells) or TEPP-46 *in vitro*, and re-stimulated them with CD3$^-$ splenocytes in the presence of MOG$_{35–55}$ and IL-1β/IL-23 cytokines. This protocol induces the generation of MOG$_{35–55}$-specific, IL-17A/IFN-γ-producing T cells able to induce EAE in C57Bl/6 recipient mice (Raverdeau et al., 2016). Our data indicate that TEPP-46-pre-treated T cells induced a less severe EAE, compared to CTRL cells, in terms of both disease severity and percentage weight loss (Figure 6F). These results confirm that specific inhibition of T cell pathogenicity with TEPP-46 is sufficient to limit the development of T cell-mediated autoimmunity.

Human CD4$^+$ T Cells Upregulate PKM2 upon TCR Stimulation and TEPP-46 Limits Their Activation

We next evaluated PKM2 expression in human CD4$^+$ T cells. Time-dependent PKM2 upregulation was observed in human naïve CD4$^+$ T cells activated with CD3/CD28 antibodies (Figures 7A and 7B). As murine cells, human CD4$^+$ T cells also upregulated PKM1 upon activation, but *PKM2* mRNA levels were higher at all time points analyzed (Figures S1D–S1F), confirming a preferential expression of PKM2 over PKM1 in CD4$^+$ T cells. We also detected an increase in Y105 phosphorylation, tetrameric and monomeric/dimeric PKM2 in activated human T cells (Figures 7C and 7D). Human CD4$^+$ T cells activation also led to increased PKM2 S37 phosphorylation as well as PKM2 nuclear accumulation in activated T cells (Figures 7E and 7F). We finally evaluated the impact of PKM2 tetramerization on human CD4$^+$ T cells activation. First, we found that treatment with TEPP-46 limited *IL2* mRNA expression and IL-2 production by human T cells 48 h upon CD3/CD28 activation, suggesting an inhibition of early T cell activation (Figures 7G and 7H). TEPP-46 also blocked human CD4$^+$ T cell proliferation and upregulation of CD71, a well-established human T cell activation marker (Figures 7I and 7J), while TNF-α production by activated human cells was not affected (data not shown). Finally, as in murine cells, PKM2 tetramerization induced the generation of FOXP3$^+$CD25^{high}CD127^{neg} human Tregs (Figure 7K). Overall, these results suggest that modulation of PKM2 activity may represent a valuable approach to limit T cell activation in human inflammatory diseases.

DISCUSSION

The metabolic reprogramming happening in lymphocytes is not a novel concept. Early studies indeed showed engagement of aerobic glycolysis in lymphocytes upon activation, which was characterized by increased expression of glycolytic enzymes that preceded the proliferative phase (Wang et al., 1976; Hume

(A) Flow cytometry evaluation of IL-17A and TNF-α production by Th17 cells after intracellular cytokine staining. Left, representative plots showing reduced IL-17A and TNF-α production by TEPP-46 treated cells. Right, quantification of the percentage of IL-17A/TNF-α-producing cells and of IL-17A/TNF-α MFI in CTRL versus TEPP-46-treated cells (n = 6–9 from 3 independent experiments).
(B and C) Quantification of the mRNA levels of Th17 signature cytokines (B) and transcription factors (C) by qRT-PCR (n = 6–8 from 3–4 independent experiments). For all panels, data are the mean ± SD. *p < 0.05, **p < 0.01, ***p < 0.001, or ****p < 0.0001 compared to CTRL condition, by one-way ANOVA with Dunnett's post-hoc test.

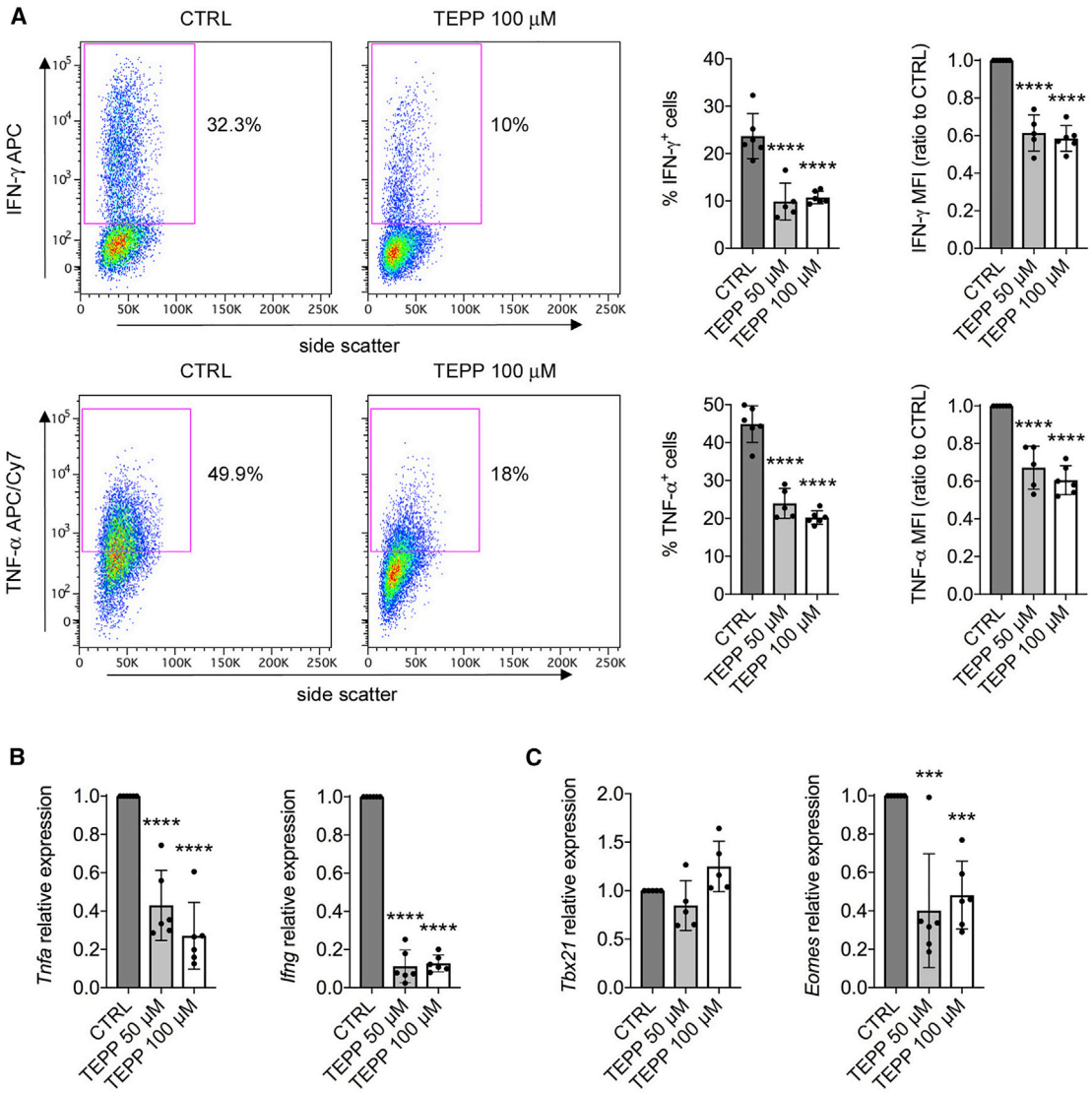

Figure 5. TEPP-46 Constrains Th1 Cell Development

Murine CD4$^+$CD62$^+$ T cells were activated *in vitro* for 3 days with CD3/CD28 antibodies under Th1-polarizing conditions in the presence of DMSO (CTRL condition) or TEPP-46 50 μM or 100 μM.

(A) Flow cytometry evaluation of IFN-γ and TNF-α production by Th1 cells after intracellular cytokine staining. Left, representative plots showing reduced IFN-γ and TNF-α production by TEPP-46 treated cells. Right, quantification of the percentage of IFN-γ/TNF-α-producing cells and of IFN-γ/TNF-α MFI in CTRL versus TEPP-46-treated cells (n = 5–6 from 4 independent experiments).

(B and C) Quantification of *Tnfa*/*Ifng* (B) and *Tbx21*/*Eomes* (C) mRNA levels by qPCR (n = 5–6 from 3 independent experiments). For all panels, data are the mean ± SD. ***p < 0.001 or ****p < 0.0001 compared to CTRL condition, by one-way ANOVA with Dunnett's post-hoc test.

et al., 1978; Marjanovic et al., 1991). Among these, previous work showed that, upon TCR stimulation, T cells upregulate PKM2 expression (Wang et al., 2011; Cao et al., 2014). Furthermore, a study has shown that PKM2 controls T cell activation induced by homocysteine (Lü et al., 2018). However, the possibility of controlling T cell activation by modulating PKM2 activity and isomerization pharmacologically was never investigated thus far, particularly in the context of T cell subsets. In this study, we report that PKM2 is upregulated and accumulates in the nucleus of CD4$^+$ T cells upon TCR engagement. We show that promotion of PKM2 tetramerization and inhibition of PKM2 nuclear translocation by a small molecule pharmacological activator termed TEPP-46 severely impacts T cell activation, constrains the development of pro-inflammatory Th17 and Th1 cells *in vitro*, and inhibits T cell-mediated neuroinflammation *in vivo*.

In the present manuscript, we report that both murine and human CD4$^+$ T cells also upregulate the expression of the PKM1 isoform upon activation. However, T cells preferentially express PKM2 over PKM1 both in resting conditions and upon activation, in agreement with data from an early report suggesting a preferential expression of PKM2 over PKM1 in rat

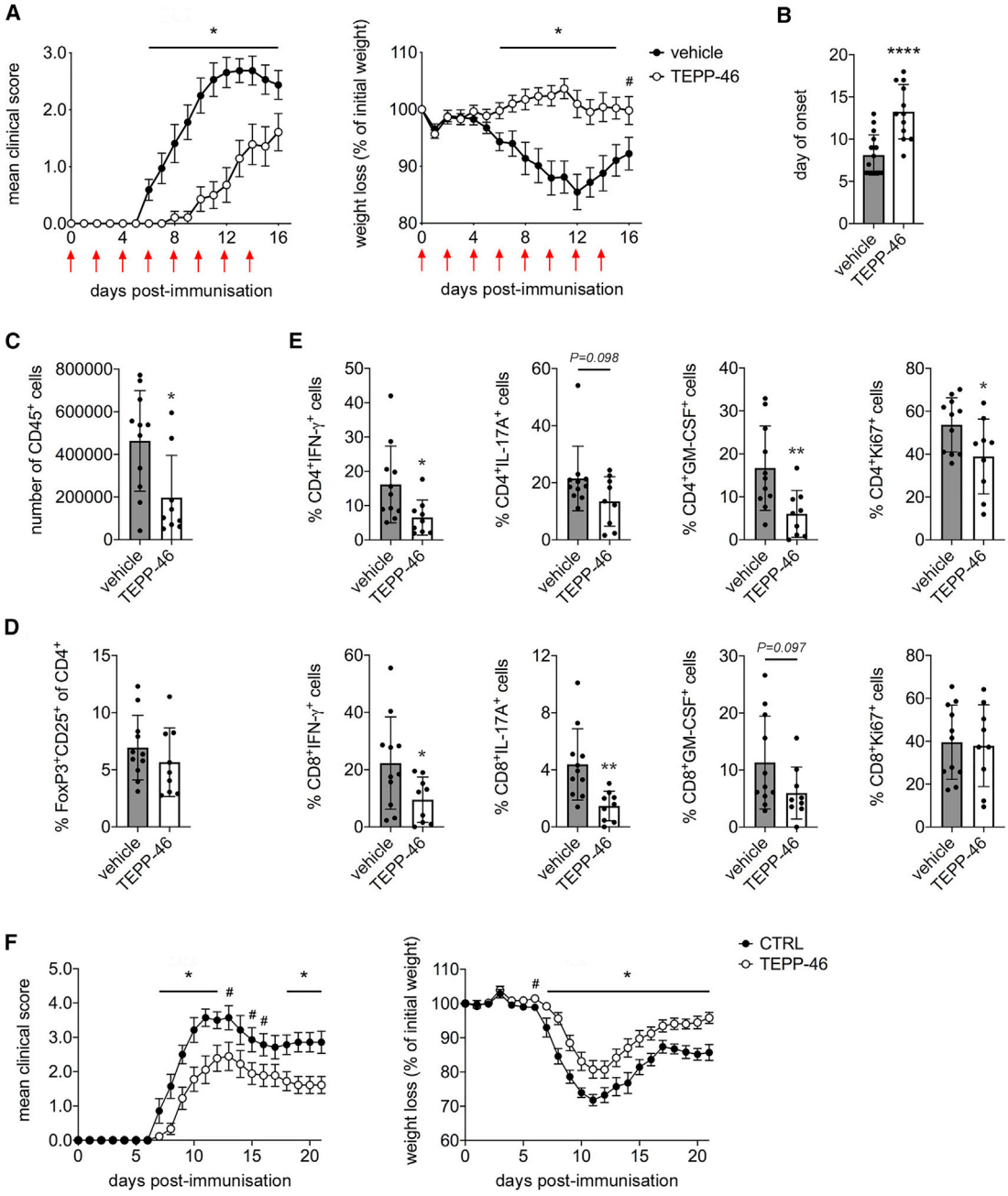

Figure 6. TEPP-46 Inhibits EAE Development

(A and B) C56Bl/6 mice were immunized with $MOG_{35–55}$ peptide emulsified in complete Freund adjuvant. Mice were treated every other day from day 0 to day +14 post-immunization (red arrows) with vehicle (PBS + 40% cyclodextrin) or TEPP-46 50 mg/kg in vehicle.

(A) Mean clinical score (left) and percentage of weight loss (right) in EAE mice treated with vehicle or TEPP-46.

(B) Mean day of onset in vehicle and TEPP-46-treated EAE mice. N = 14–16 mice per group (A) or 12–16 mice/group (B) from 3 independent experiments.

(C–E) Vehicle- and TEPP-46-treated EAE mice were sacrificed 11 days post-immunization. CNS infiltrates were isolated, stained, and analyzed by flow cytometry as described in the STAR Methods section.

(C) Total number of $CD45^+$ cells in the CNS of vehicle- and TEPP-46-treated EAE mice.

(D) Percentage of $Foxp3^+CD25^+$ cells in the $CD4^+$ T cells population isolated from the CNS of EAE mice.

(E) Percentages of IL-17A-, IFN-γ-, and GM-CSF-producing and $Ki67^+$ cells in the CNS $CD4^+$ and $CD8^+$ T populations of vehicle and TEPP-46-treated mice. For (C–E), n = 9–11 from 2 independent experiments.

(F) Transfer EAE was induced in C57BL/6 mice by injection of $MOG_{35–55}$-primed $CD3^+$ T cells re-stimulated *in vitro* as described in STAR Methods section. N = 7–9 mice/group from 2 independent experiments. For panels (A) and (F), data are the mean ± standard error of the mean (SEM). For panels (B–E), data are the mean ± SD. p values were calculated by two-tailed unpaired Student's t test. $^{\#}p < 0.01$, $^{*}p < 0.05$, and $^{****}p < 0.0001$, compared to vehicle condition (A–E) or CTRL cell condition (F).

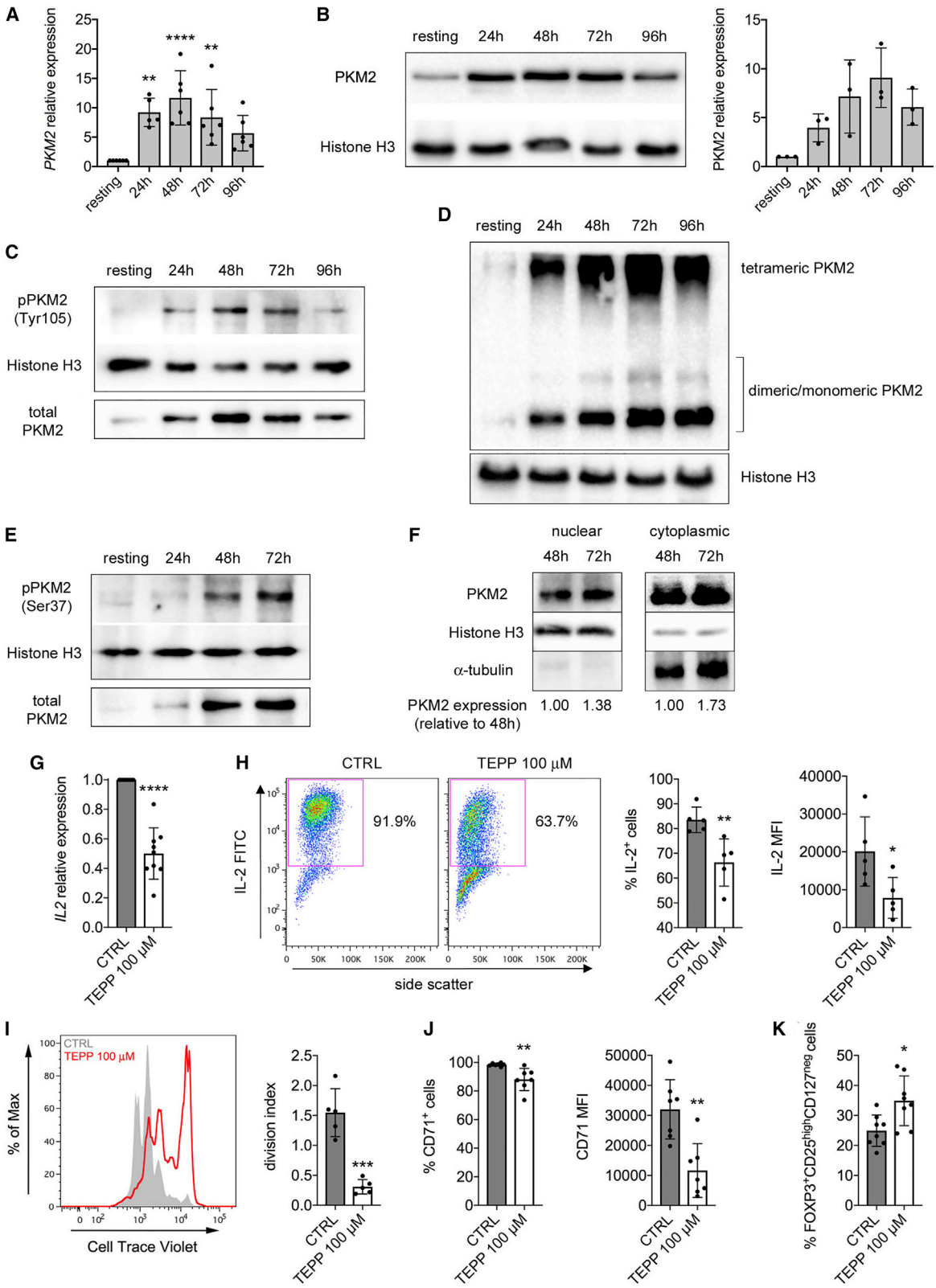

Figure 7. TCR Stimulation Induces PKM2 Upregulation and Nuclear Translocation in Human T Cells, and TEPP-46 Limits Their Activation

Human naive CD4$^+$ T cells were stimulated *in vitro* for 4 days with CD3/CD28 antibodies and collected at different time points of activation.

(A) Quantification of *PKM2* mRNA in resting versus activated human CD4$^+$ T cells by qRT-PCR (n = 5–6 from three independent experiments).

(legend continued on next page)

thymocytes (Netzker et al., 1992). Nonetheless, PKM1 upregulation upon CD3/CD28 activation is of interest. These results are somewhat surprising, as PKM1 and PKM2 expression is usually inversely correlated in immune cells. In particular, we previously reported that bone marrow-derived macrophages express PKM1 in resting conditions, while upregulating PKM2 and downregulating PKM1 upon lipopolysaccharide (LPS) activation (Palsson-McDermott et al., 2015). Of note, transformed cells preferentially express PKM2 for their anabolic metabolism, and exogenous expression of the PKM1 isoforms is normally associated with a block in tumor growth (Israelsen and Vander Heiden, 2015). For these reasons, we speculate that PKM1 is likely to play a different role than PKM2 during T cell activation. However, further studies are required to shed light on this aspect.

Dimeric PKM2 has been proposed to translocate to the nucleus of proliferating cells, exerting different functions, such as histone phosphorylation and regulation of gene transcription, including control of *Myc* transcription and interaction with HIF-1α to boost expression of HIF-1α-dependent genes, such as those encoding enzymes involved in glycolysis (Israelsen and Vander Heiden, 2015; Palsson-McDermott et al., 2015; Lunt et al., 2015; Prakasam et al., 2018; Yang et al., 2012b; Gao et al., 2012). Dimeric PKM2 has also been shown to modulate the activity of mTORC1 in transformed cells, via phosphorylation of the mTORC1 inhibitor proline-rich AKT1 substrate 1 (AKT1S1) (He et al., 2016) or by reducing serine synthesis, which was shown to sustain mTORC1 function in proliferating cells (Ye et al., 2012). Our data suggest that PKM2 "moonlighting" activity may control the functionality of HIF-1α, mTORC1, and Myc and the engagement of aerobic glycolysis in TCR-activated $CD4^+$ T cells, which are crucial determinants for their activation and effector functions (Geltink et al., 2018). However, further studies are needed to evaluate if monomeric/dimeric PKM2 directly interact with HIF-1α and mTORC1 or specifically control *Myc* gene expression in activated T cells. Of note, the levels of PKM2 in the nucleus are low in resting T cells, and previous work indicates that HIF-1α and Myc activity may be controlled by mTORC1 itself (Csibi et al., 2014; Wei et al., 2016; Düvel et al., 2010; Shi et al., 2011). Upregulation and maintenance of high expression levels of HIF-1α and Myc upon CD3/CD28 stimulation might therefore be blocked by inhibition of both the nuclear activity of PKM2 and the inhibitory effect on mTORC1 in the cytoplasm induced by PKM2 tetramerization. These results would explain why TEPP-46 inhibits the induction of glycolysis in T cells, acting to limit expression of glycolytic enzymes and block mTORC1 activity. Interestingly, we found that TEPP-46-treated T cells did not affect OCR in activated T cells, confirming that TEPP-46 specifically impact the engagement of glycolysis in T cells. Of note, while blocking PKM2 translocation into the nucleus and induction of glycolytic gene, TEPP-46 also increases the activity of PKM2 by inducing its tetramerization (Anastasiou et al., 2012). This would likely maintain a constant rate of pyruvate flux into the TCA cycle and may be the reason why OCR is not affected by TEPP-46. Importantly, previous work in transformed cells, as well as in immune cells, suggest that, apart from glycolysis, induction of PKM2 tetramerization or knock down of the PKM2 gene may impact engagement of PPP and nucleotide synthesis as well as lipid metabolism (Palsson-McDermott et al., 2015; Lunt et al., 2015; Lü et al., 2018; Anastasiou et al., 2012). TEPP-46 may therefore have a broader effect on T cell metabolism.

Our work also suggests that while PKM2 tetramerization constrains the development of pro-inflammatory Th17 and Th1 cells, it might favor the generation of Tregs under pro-inflammatory conditions, with a consequent inhibition of autoimmunity *in vivo*. This is supported by the inhibitory effect we observed in EAE, a well-known Th17/Th1-dependent model of autoimmunity. However, our RNA-seq data did not show induction of a global regulatory phenotype in T cells treated with TEPP-46, suggesting that the small amount of $Foxp3^+CD25^+$ T cells induced by TEPP-46 treatment might not be relevant. We also did not observe a significant induction of $Foxp3^+CD25^+$ Tregs by TEPP-46 in EAE mice, suggesting that generation of Tregs *in vivo* is not the main beneficial effect of TEPP-46 on disease development. Of note, previous work showed that inhibition of mTORC1, Myc, and HIF-1α all induce the development of $Foxp3^+$ T cells under inflammatory conditions, mainly by blocking the engagement of glycolysis (Wei et al., 2016; Shi et al., 2011; Dang et al., 2011; Feldhoff et al., 2017). However, other studies have shown that glycolysis and mTORC1/HIF-1α activity could favor the

(B) Left, western blot showing upregulation of PKM2 protein in human $CD4^+$ cells following activation. Right, quantification of PKM2 expression by densitometry analysis (n = 3 from 2 independent experiments).
(C) Western blots showing time-dependent increase in PKM2 phosphorylation on Tyr105 in activated human T cells. One representative experiment out of two is shown.
(D) Cells were collected at different time points of activation, crosslinked with DSS, and analyzed for PKM2 expression by western blot. A representative blot showing the upregulation of monomeric/dimeric and tetrameric PKM2 in activated human $CD4^+$ T cells is presented.
(E) Western blots showing time-dependent increase in PKM2 phosphorylation on Ser37 in activated human $CD4^+$ T cells.
(F) Cells were collected at different time points of activation. Nuclear and cytoplasmic fractions were isolated by cell fractionation and analyzed for PKM2 expression by western blot. A representative blot showing accumulation of PKM2 in the nucleus of activated human $CD4^+$ T cells is presented. For (D–F), one representative experiment out of three is shown.
(G–K) Human naïve $CD4^+$ T cells were stimulated *in vitro* for 48 h (G and H) or 4 days (I–K) with CD3/CD28 antibodies, in the presence of DMSO (CTRL condition) or TEPP-46 100 μM.
(G) Quantification of *IL2* mRNA in activated human cells by qRT-PCR (n = 9 from five independent experiments).
(H) IL-2 production evaluated by flow cytometry after intracellular cytokine staining. Left, representative plot showing reduced IL-2 production by TEPP-46 treated cells. Right, quantification of the percentage of IL-2-producing cells and IL-2 MFI in CTRL versus TEPP-46-treated cells (n = 5 from 3 independent experiments).
(I) Human $CD4^+$ T cells proliferation evaluated as in Figure 2C (n = 5 from 2 independent experiments).
(J) Percentage of $CD71^+$ cells (left) and CD71 MFI (right) in CTRL and TEPP-46-treated activated human T cells (n = 7 from three independent experiments).
(K) Percentage of $FOXP3^+CD25^{high}CD127^{neg}$ cells in CTRL and TEPP-46-treated activated $CD4^+$ human T cells (n = 8 from 3 independent experiments). For all panels, data are the mean ± SD. *p < 0.05, **p < 0.01, ***p < 0.001, or ****p<0.0001, compared to CTRL condition. p values were calculated by one-way ANOVA with Dunnett's post-hoc test (A) or by two-tailed paired (G) or unpaired (H–K) Student's t test.

generation of Tregs, especially *in vivo* (Clambey et al., 2012; Zeng et al., 2013; Wu et al., 2014; Procaccini et al., 2016). Overall, the specific role of glycolysis in Tregs is indeed less clear than in conventional T cells. Considering our results showing that TEPP-46 blocks the induction of Tregs by TGF-β *in vitro*, further studies are needed to evaluate the importance of PKM2 in Treg generation and functionality. Interestingly, we also observed that PKM2 tetramerization specifically modulated the expression of certain Th17- and Th1-specific transcription factors (*Rora*, *Irf4*, *Runx1,* and *Eomes*), without affecting other subset signature genes, such as *Rorc* and *Tbx21*, under Th17- and Th1-polarizing conditions. HIF-1α and mTOR activity was previously shown to control T helper cell differentiation, but the specific role of such master regulators in the expression of lineage-specific transcription factors is not well understood. For example, previous work suggested that HIF-1α activity directly controls *Rorc* transcription in Th17 cells (Dang et al., 2011). However, Shi et al. showed that the block in Th17 development in HIF-1α knockout T cells was not caused by downregulation of *Rorc* expression (Shi et al., 2011). Similarly, lack of mTOR activity was reported to inhibit Th1 and Th17 cell development and induction of *Tbet* and *Rorc* under Th1- and Th17-polarizing conditions (Delgoffe et al., 2009), but Chang et al. showed that mTOR activity is essential for Th17 cell development without controlling the expression of *Rorc* (Chang et al., 2013). Our work suggests that PKM2 tetramerization induces a complex regulation of transcription factor expression in T helper cell subsets, but future studies are required to determine whether PKM2 directly regulates the expression of these transcription factors, or if the observed TEPP-46-mediated effects are indirect through the initial block in glycolysis and Myc/HIF-1α/mTOR signaling.

Our data indicate that PKM2 may modulate the generation of different cell subsets by affecting signal transducer and activator of transcription (STAT) proteins. STATs are essential players in the polarization of pro-inflammatory T cell subsets, with STAT3 being crucial for Th17 development, STAT1/STAT4 controlling Th1 generation and STAT5 regulating induction of Tregs by TGF-β (Seif et al., 2017). Interestingly, Lochmatter and colleagues showed that IL-23, a cytokine important for Th17 polarization, causes PKM2 nuclear translocation with associated increased STAT3 phosphorylation in T cells, although a formal demonstration of direct STAT3 phosphorylation by PKM2 was not provided (Lochmatter et al., 2016). However, dimeric PKM2 was previously reported to translocate to the nucleus of cancer cells, where it could directly phosphorylate STAT3, inducing the expression of STAT3-dependent genes (Gao et al., 2012). Moreover, a recent study linked PKM2 to STAT1 in bone marrow-derived macrophages, suggesting that PKM2 may also regulate STAT1 activity (Deng et al., 2018). Finally, nuclear PKM2 was shown to regulate STAT5 activity in cancer cells (Park et al., 2016). Of note, while PKM2 protein kinase activity was previously questioned (Hosios et al., 2015), a recent work demonstrated that PKM2 could phosphorylate protein substrates, confirming the potential of such an enzyme to regulate protein functions by post-transcriptional phosphorylation (He et al., 2016). In this paper, we demonstrate that PKM2 may control STAT5 phosphorylation induced by TFG-β and the generation of Tregs *in vitro*. Whether this is due to direct phosphorylation of STAT5 by monomeric/dimeric PKM2 remains to be determined. However, we did not observe any effect of TEPP-46 on the phosphorylation of STAT3 in Th17 cells or STAT1 in Th1 cells (data not shown). Interestingly, preliminary results suggest that TEPP-46 reduces STAT4 expression, and consequently the amount of phosphorylated STAT4, in Th1-polarized cells (data not shown), and we are currently investigating the basis of STAT4 regulation by PKM2 in such a T cell subset.

In conclusion, our work demonstrates that impacting the moonlighting activity of PKM2 may represent a valuable approach to limit T cell activation and pathogenicity. Inhibition of aerobic glycolysis was previously shown to limit Th17 generation and development of T cell-mediated autoimmunity in mouse models and human disease (Shi et al., 2011; Bian et al., 2009; Gerriets et al., 2015; Kornberg et al., 2018), and our paper supports the idea that modulation of T cell intracellular metabolism represents a valuable therapeutic approach in inflammation. Notably, during the revision process of the present manuscript, Kono et al. supported a role for PKM2 in the generation of Th1 and Th17 cells, with blocking or knock down of PKM2 in T cells limiting Th1/Th17 development and being beneficial in EAE (Kono et al., 2019). Given our previous report showing inhibition of inflammatory macrophage activation by TEPP-46 (Palsson-McDermott et al., 2015), we propose that induction of PKM2 tetramerization by small molecule activators may have therapeutic utility in inflammatory pathologies and autoimmune disease.

Limitations of Study

Our study suggests that PKM2 moonlighting functions control $CD4^+$ T cell activation and development of Th17 and Th1 cells both *in vitro* and *in vivo*. Additional studies should focus on which precise functions of PKM2 are involved here, such as effects in the nucleus or protein kinase activity, and further analysis of the role played by metabolic alterations. To further confirm a role for PKM2 in T cell activation and pathogenicity, the effect of PKM2 genetic deletion on T cell functionality, which has previously been shown to inhibit IFN-γ production and Th17 development in different settings (Lü et al., 2018; Kono et al., 2019), should be analyzed in both murine and human $CD4^+$ T cells. Such analyses will further confirm the role of PKM2 in $CD4^+$ T cell function in health and disease.

STAR★METHODS

Detailed methods are provided in the online version of this paper and include the following:

- KEY RESOURCES TABLE
- LEAD CONTACT AND MATERIALS AVAILABILITY
- EXPERIMENTAL MODEL AND SUBJECT DETAILS
  - Mice
  - Human Samples
- METHOD DETAILS
  - Cell Isolation and Cultures
  - Nuclear Extraction, PKM2 Crosslinking, and Western Blotting
  - Quantitative Real-Time PCR (qRT-PCR)
  - Flow Cytometry

SUPPLEMENTAL INFORMATION

Supplemental Information can be found online at https://doi.org/10.1016/j.cmet.2019.10.015.

ACKNOWLEDGMENTS

We thank Craig J. Thomas and Scott B. Hoyt from the Division of Preclinical Innovations at the National Center for Advancing Translational Sciences (National Institutes of Health; Bethesda, Maryland, USA) for providing TEPP-46. This work was supported by a Marie Skłodowska-Curie Individual Fellowship from the European Commission (to S.A.; grant code: 796507); by Wellcome Trust, UK (to L.A.J.O.; grant number: 205455); by Science Foundation Ireland (SFI Investigator award 16/IA/4468 to K.H.G.M.); and by the Max Planck Society (to E.L.P.).

AUTHOR CONTRIBUTIONS

S.A. performed most of the experiments and analyzed all data. E.M.P-M., M.C.R., G.P., and H.K. assisted with *in vitro* experiments. S.A. and C.E.S. performed EAE experiments. B.K., M.C.R., and N.R. performed the analysis of RNA-seq data. E.L.P. and K.H.G.M. provided critical input. L.A.J.O. oversaw the project. S.A. and L.A.J.O. conceived the study and wrote the manuscript.

DECLARATION OF INTERESTS

L.A.J.O. is a Founder of Sitryx. E.L.P. is a Scientific Advisory Board member of ImmunoMet and a Founder of Rheos Medicines.

Received: May 8, 2019
Revised: September 28, 2019
Accepted: October 29, 2019
Published: November 21, 2019

REFERENCES

Anastasiou, D., Yu, Y., Israelsen, W.J., Jiang, J.K., Boxer, M.B., Hong, B.S., Tempel, W., Dimov, S., Shen, M., Jha, A., et al. (2012). Pyruvate kinase M2 activators promote tetramer formation and suppress tumorigenesis. Nat. Chem. Biol. *8*, 839–847.

Bettencourt, I.A., and Powell, J.D. (2017). Targeting metabolism as a novel therapeutic approach to autoimmunity, inflammation, and transplantation. J. Immunol. *198*, 999–1005.

Bhardwaj, V., Heyne, S., Sikora, K., Rabbani, L., Rauer, M., Kilpert, F., Richter, A.S., Ryan, D., and Manke, T. (2019). snakePipes: facilitating flexible, scalable and integrative epigenomic analysis. Bioinformatics *35*, 4757–4759.

Bian, L., Josefsson, E., Jonsson, I.M., Verdrengh, M., Ohlsson, C., Bokarewa, M., Tarkowski, A., and Magnusson, M. (2009). Dichloroacetate alleviates development of collagen II-induced arthritis in female DBA/1 mice. Arthritis Res. Ther. *11*, R132.

Cao, Y., Rathmell, J.C., and Macintyre, A.N. (2014). Metabolic reprogramming towards aerobic glycolysis correlates with greater proliferative ability and resistance to metabolic inhibition in CD8 versus CD4 T cells. PLoS One *9*, e104104.

Chang, J., Burkett, P.R., Borges, C.M., Kuchroo, V.K., Turka, L.A., and Chang, C.H. (2013). MyD88 is essential to sustain mTOR activation necessary to promote T helper 17 cell proliferation by linking IL-1 and IL-23 signaling. Proc. Natl. Acad. Sci. USA *110*, 2270–2275.

Clambey, E.T., McNamee, E.N., Westrich, J.A., Glover, L.E., Campbell, E.L., Jedlicka, P., de Zoeten, E.F., Cambier, J.C., Stenmark, K.R., Colgan, S.P., et al. (2012). Hypoxia-inducible factor-1 alpha-dependent induction of FoxP3 drives regulatory T-cell abundance and function during inflammatory hypoxia of the mucosa. Proc. Natl. Acad. Sci. USA *109*, E2784–E2793.

Csibi, A., Lee, G., Yoon, S.O., Tong, H., Ilter, D., Elia, I., Fendt, S.M., Roberts, T.M., and Blenis, J. (2014). The mTORC1/S6K1 pathway regulates glutamine metabolism through the eIF4B-dependent control of c-Myc translation. Curr. Biol. *24*, 2274–2280.

Dang, E.V., Barbi, J., Yang, H.Y., Jinasena, D., Yu, H., Zheng, Y., Bordman, Z., Fu, J., Kim, Y., Yen, H.R., et al. (2011). Control of T(H)17/T(reg) balance by hypoxia-inducible factor 1. Cell *146*, 772–784.

Dayton, T.L., Jacks, T., and Vander Heiden, M.G. (2016). PKM2, cancer metabolism, and the road ahead. EMBO Rep. *17*, 1721–1730.

Delgoffe, G.M., Kole, T.P., Zheng, Y., Zarek, P.E., Matthews, K.L., Xiao, B., Worley, P.F., Kozma, S.C., and Powell, J.D. (2009). The mTOR kinase differentially regulates effector and regulatory T cell lineage commitment. Immunity *30*, 832–844.

Deng, W., Zhu, S., Zeng, L., Liu, J., Kang, R., Yang, M., Cao, L., Wang, H., Billiar, T.R., Jiang, J., et al. (2018). The circadian clock controls immune checkpoint pathway in sepsis. Cell Rep. *24*, 366–378.

Dobin, A., Davis, C.A., Schlesinger, F., Drenkow, J., Zaleski, C., Jha, S., Batut, P., Chaisson, M., and Gingeras, T.R. (2013). STAR: ultrafast universal RNA-seq aligner. Bioinformatics *29*, 15–21.

Dong, G., Mao, Q., Xia, W., Xu, Y., Wang, J., Xu, L., and Jiang, F. (2016). PKM2 and cancer: the function of PKM2 beyond glycolysis. Oncol. Lett. *11*, 1980–1986.

Düvel, K., Yecies, J.L., Menon, S., Raman, P., Lipovsky, A.I., Souza, A.L., Triantafellow, E., Ma, Q., Gorski, R., Cleaver, S., et al. (2010). Activation of a metabolic gene regulatory network downstream of mTOR complex 1. Mol. Cell *39*, 171–183.

Feldhoff, L.M., Rueda, C.M., Moreno-Fernandez, M.E., Sauer, J., Jackson, C.M., Chougnet, C.A., and Rupp, J. (2017). IL-1β induced HIF-1α inhibits the differentiation of human FOXP3+ T cells. Sci. Rep. *7*, 465.

Freitag, J., Berod, L., Kamradt, T., and Sparwasser, T. (2016). Immunometabolism and autoimmunity. Immunol. Cell Biol. *94*, 925–934.

Gao, X., Wang, H., Yang, J.J., Liu, X., and Liu, Z.R. (2012). Pyruvate kinase M2 regulates gene transcription by acting as a protein kinase. Mol. Cell *45*, 598–609.

Geltink, R.I.K., Kyle, R.L., and Pearce, E.L. (2018). Unraveling the complex interplay between T cell metabolism and function. Annu. Rev. Immunol. *36*, 461–488.

Gerriets, V.A., Kishton, R.J., Nichols, A.G., Macintyre, A.N., Inoue, M., Ilkayeva, O., Winter, P.S., Liu, X., Priyadharshini, B., Slawinska, M.E., et al. (2015). Metabolic programming and PDHK1 control CD4+ T cell subsets and inflammation. J. Clin. Invest. *125*, 194–207.

Hawkins, E.D., Hommel, M., Turner, M.L., Battye, F.L., Markham, J.F., and Hodgkin, P.D. (2007). Measuring lymphocyte proliferation, survival and differentiation using CFSE time-series data. Nat. Protoc. *2*, 2057–2067.

He, C.L., Bian, Y.Y., Xue, Y., Liu, Z.X., Zhou, K.Q., Yao, C.F., Lin, Y., Zou, H.F., Luo, F.X., Qu, Y.Y., et al. (2016). Pyruvate kinase M2 activates mTORC1 by phosphorylating AKT1S1. Sci. Rep. *6*, 21524.

Hitosugi, T., Kang, S., Vander Heiden, M.G., Chung, T.W., Elf, S., Lythgoe, K., Dong, S., Lonial, S., Wang, X., Chen, G.Z., et al. (2009). Tyrosine phosphorylation inhibits PKM2 to promote the Warburg effect and tumor growth. Sci. Signal. *2*, ra73.

Hosios, A.M., Fiske, B.P., Gui, D.Y., and Vander Heiden, M.G. (2015). Lack of evidence for PKM2 protein kinase activity. Mol. Cell *59*, 850–857.

Hume, D.A., Radik, J.L., Ferber, E., and Weidemann, M.J. (1978). Aerobic glycolysis and lymphocyte transformation. Biochem. J. *174*, 703–709.

Israelsen, W.J., and Vander Heiden, M.G. (2015). Pyruvate kinase: function, regulation and role in cancer. Semin. Cell Dev. Biol. *43*, 43–51.

Kipp, M., Nyamoya, S., Hochstrasser, T., and Amor, S. (2017). Multiple sclerosis animal models: a clinical and histopathological perspective. Brain Pathol. *27*, 123–137.

Kono, M., Maeda, K., Stocton-Gavanescu, I., Pan, W., Umeda, M., Katsuyama, E., Burbano, C., Orite, S.Y.K., Vukelic, M., Tsokos, M.G., et al. (2019). Pyruvate kinase M2 is requisite for Th1 and Th17 differentiation. JCI Insight *4*, 12.

Kornberg, M.D., Bhargava, P., Kim, P.M., Putluri, V., Snowman, A.M., Putluri, N., Calabresi, P.A., and Snyder, S.H. (2018). Dimethyl fumarate targets GAPDH and aerobic glycolysis to modulate immunity. Science *360*, 449–453.

Kostic, M., Zivkovic, N., Cvetanovic, A., and Stojanovic, I. (2018). Granulocyte-macrophage colony-stimulating factor as a mediator of autoimmunity in multiple sclerosis. J. Neuroimmunol. *323*, 1–9.

Liao, Y., Smyth, G.K., and Shi, W. (2014). featureCounts: an efficient general purpose program for assigning sequence reads to genomic features. Bioinformatics *30*, 923–930.

Lochmatter, C., Fischer, R., Charles, P.D., Yu, Z., Powrie, F., and Kessler, B.M. (2016). Integrative phosphoproteomics links IL-23R signaling with metabolic adaptation in lymphocytes. Sci. Rep. *6*, 24491.

Love, M.I., Huber, W., and Anders, S. (2014). Moderated estimation of fold change and dispersion for RNA-seq data with DESeq2. Genome Biol. *15*, 550.

Lü, S., Deng, J., Liu, H., Liu, B., Yang, J., Miao, Y., Li, J., Wang, N., Jiang, C., Xu, Q., et al. (2018). PKM2-dependent metabolic reprogramming in $CD4^+$ T cells is crucial for hyperhomocysteinemia-accelerated atherosclerosis. J. Mol. Med. (Berl.) *96*, 585–600.

Lunt, S.Y., Muralidhar, V., Hosios, A.M., Israelsen, W.J., Gui, D.Y., Newhouse, L., Ogrodzinski, M., Hecht, V., Xu, K., Acevedo, P.N., et al. (2015). Pyruvate kinase isoform expression alters nucleotide synthesis to impact cell proliferation. Mol. Cell *57*, 95–107.

Luo, W., Hu, H., Chang, R., Zhong, J., Knabel, M., O'Meally, R., Cole, R.N., Pandey, A., and Semenza, G.L. (2011). Pyruvate kinase M2 is a PHD3-stimulated coactivator for hypoxia-inducible factor 1. Cell *145*, 732–744.

Macintyre, A.N., Gerriets, V.A., Nichols, A.G., Michalek, R.D., Rudolph, M.C., Deoliveira, D., Anderson, S.M., Abel, E.D., Chen, B.J., Hale, L.P., et al. (2014). The glucose transporter Glut1 is selectively essential for CD4 T cell activation and effector function. Cell Metab. *20*, 61–72.

Mähler Convenor, M., Berard, M., Feinstein, R., Gallagher, A., Illgen-Wilcke, B., Pritchett-Corning, K., and Raspa, M. (2014). FELASA recommendations for the health monitoring of mouse, rat, hamster, guinea pig and rabbit colonies in breeding and experimental units. Lab. Anim. *48*, 178–192.

Marjanovic, S., Skog, S., Heiden, T., Tribukait, B., and Nelson, B.D. (1991). Expression of glycolytic isoenzymes in activated human peripheral lymphocytes: cell cycle analysis using flow cytometry. Exp. Cell Res. *193*, 425–431.

Netzker, R., Greiner, E., Eigenbrodt, E., Noguchi, T., Tanaka, T., and Brand, K. (1992). Cell cycle-associated expression of M2-type isozyme of pyruvate kinase in proliferating rat thymocytes. J. Biol. Chem. *267*, 6421–6424.

O'Neill, L.A., Kishton, R.J., and Rathmell, J. (2016). A guide to immunometabolism for immunologists. Nat. Rev. Immunol. *16*, 553–565.

Palsson-McDermott, E.M., Curtis, A.M., Goel, G., Lauterbach, M.R., Sheedy, F.J., Gleeson, L.E., van den Bosch, M.M., Quinn, S.R., Domingo-Fernandez, R., Johnston, D.W., et al. (2015). Pyruvate kinase M2 regulates HIF-1α activity and IL-1β induction and is a critical determinant of the warburg effect in LPS-activated macrophages. Cell Metab. *21*, 65–80.

Park, Y.S., Kim, D.J., Koo, H., Jang, S.H., You, Y.M., Cho, J.H., Yang, S.J., Yu, E.S., Jung, Y., Lee, D.C., et al. (2016). AKT-induced PKM2 phosphorylation signals for IGF-1-stimulated cancer cell growth. Oncotarget *7*, 48155–48167.

Pearce, E.L., and Pearce, E.J. (2013). Metabolic pathways in immune cell activation and quiescence. Immunity *38*, 633–643.

Prakasam, G., Iqbal, M.A., Bamezai, R.N.K., and Mazurek, S. (2018). Posttranslational modifications of pyruvate kinase M2: tweaks that benefit cancer. Front. Oncol. *8*, 22.

Procaccini, C., Carbone, F., Di Silvestre, D., Brambilla, F., De Rosa, V., Galgani, M., Faicchia, D., Marone, G., Tramontano, D., Corona, M., et al. (2016). The proteomic landscape of human ex vivo regulatory and conventional T cells reveals specific metabolic requirements. Immunity *44*, 406–421.

Raverdeau, M., Breen, C.J., Misiak, A., and Mills, K.H. (2016). Retinoic acid suppresses IL-17 production and pathogenic activity of $\gamma\delta$ T cells in CNS autoimmunity. Immunol. Cell Biol. *94*, 763–773.

Seif, F., Khoshmirsafa, M., Aazami, H., Mohsenzadegan, M., Sedighi, G., and Bahar, M. (2017). The role of JAK-STAT signaling pathway and its regulators in the fate of T helper cells. Cell Commun. Signal. *15*, 23.

Shi, L.Z., Wang, R., Huang, G., Vogel, P., Neale, G., Green, D.R., and Chi, H. (2011). HIF1alpha-dependent glycolytic pathway orchestrates a metabolic checkpoint for the differentiation of TH17 and Treg cells. J. Exp. Med. *208*, 1367–1376.

Sutton, C.E., Finlay, C.M., Raverdeau, M., Early, J.O., DeCourcey, J., Zaslona, Z., O'Neill, L.A.J., Mills, K.H.G., and Curtis, A.M. (2017). Loss of the molecular clock in myeloid cells exacerbates T cell-mediated CNS autoimmune disease. Nat. Commun. *8*, 1923.

Wang, R., Dillon, C.P., Shi, L.Z., Milasta, S., Carter, R., Finkelstein, D., McCormick, L.L., Fitzgerald, P., Chi, H., Munger, J., et al. (2011). The transcription factor Myc controls metabolic reprogramming upon T lymphocyte activation. Immunity *35*, 871–882.

Wang, T., Marquardt, C., and Foker, J. (1976). Aerobic glycolysis during lymphocyte proliferation. Nature *261*, 702–705.

Wei, J., Long, L., Yang, K., Guy, C., Shrestha, S., Chen, Z., Wu, C., Vogel, P., Neale, G., Green, D.R., et al. (2016). Autophagy enforces functional integrity of regulatory T cells by coupling environmental cues and metabolic homeostasis. Nat. Immunol. *17*, 277–285.

Wu, J., Cui, H., Zhu, Z., Wang, L., Li, H., and Wang, D. (2014). Effect of HIF1α on Foxp3 expression in CD4+ CD25- T lymphocytes. Microbiol. Immunol. *58*, 409–415.

Yang, W., Xia, Y., Hawke, D., Li, X., Liang, J., Xing, D., Aldape, K., Hunter, T., Yung, W.K.A., and Lu, Z. (2012b). PKM2 phosphorylates histone H3 and promotes gene transcription and tumorigenesis. Cell *158*, 685–696.

Yang, W., Zheng, Y., Xia, Y., Ji, H., Chen, X., Guo, F., Lyssiotis, C.A., Aldape, K., Cantley, L.C., and Lu, Z. (2012a). ERK1/2-dependent phosphorylation and nuclear translocation of PKM2 promotes the Warburg effect. Nat. Cell Biol. *14*, 1295–1304.

Yang, Y., Xu, J., Niu, Y., Bromberg, J.S., and Ding, Y. (2008). T-bet and eomesodermin play critical roles in directing T cell differentiation to Th1 versus Th17. J. Immunol. *181*, 8700–8710.

Ye, J., Mancuso, A., Tong, X., Ward, P.S., Fan, J., Rabinowitz, J.D., and Thompson, C.B. (2012). Pyruvate kinase M2 promotes de novo serine synthesis to sustain mTORC1 activity and cell proliferation. Proc. Natl. Acad. Sci. USA *109*, 6904–6909.

Zeng, H., Yang, K., Cloer, C., Neale, G., Vogel, P., and Chi, H. (2013). mTORC1 couples immune signals and metabolic programming to establish T(reg)-cell function. Nature *499*, 485–490.

STAR★METHODS

KEY RESOURCES TABLE

REAGENT or RESOURCE	SOURCE	IDENTIFIER
Antibodies		
hamster anti-mouse CD3 (clone 145-2C11)	BD Biosciences	Cat #: 553057; RRID:AB_394590
hamster anti-mouse CD28 (clone 37.51)	Tonbo Biosciences	Cat #: 70-0281; RRID:AB_2621492
rat anti-mouse IL-4 (clone 11B11)	BD Biosciences	Cat #: 554432; RRID:AB_395388
rat anti-mouse IFN-γ (clone XMG1.2)	BD Biosciences	Cat #: 554408; RRID:AB_395373
rat anti-mouse CD62L-PE (clone MEL-14), eBioscience	Invitrogen	Cat #: 12-0621-92
rat anti-mouse CD44-PE/Cy5 (clone IM7), eBioscience	Invitrogen	Cat #: 15-0441-82; RRID:AB_468749
rat anti-mouse CD25-APC/Cy7 (clone PC61)	BioLegend	Cat #: 102025; RRID:AB_830744
rat anti-mouse Foxp3-Alexa488 (clone R16-715)	BD Biosciences	Cat #: 563487; RRID:AB_2738236
rat anti-mouse IL2-FITC (clone JES6-5H4)	BioLegend	Cat #: 503805; RRID:AB_315299
rat anti-mouse IL17A-PE (clone TC11-18H10.1)	BioLegend	Cat #: 506904; RRID:AB_315464
rat anti-mouse TNF-α-APC/Cy7 (clone MP6-XT22)	BioLegend	Cat #: 506344; RRID:AB_2565953
rat anti-mouse IFN-γAPC (clone XMG1.2)	BioLegend	Cat #: 505810; RRID:AB_315404
mouse anti-human CD3 (clone UCHT1)	BD Biosciences	Cat #: 555329; RRID:AB_395736
mouse anti-human CD28 (clone CD28.2)	BD Biosciences	Cat #: 555725; RRID:AB_396068
rat anti-human CD4-APC (clone A161A1)	BioLegend	Cat #: 357407; RRID:AB_2565659
mouse anti-human IL2-FITC (clone MQ1-17H12)	BioLegend	Cat #: 500305; RRID:AB_315092
mouse anti-human TNF-α-APC/Cy7 (clone MAb11)	BioLegend	Cat #: 502943; RRID:AB_2562869
mouse anti-human CD71-PE (clone CY1G4)	BioLegend	Cat #: 334105; RRID:AB_2271603
mouse anti-human CD127-APC/Cy7 (clone A019D5)	BioLegend	Cat #: 351347; RRID:AB_2629571
mouse anti-human CD25-Alexa488 (clone BC96)	BioLegend	Cat #: 302615; RRID:AB_493044
mouse anti-human Foxp3-BV421 (clone 206D)	BioLegend	Cat #: 320123; RRID:AB_2561338
rat anti-mouse CD45-Brilliant Violet 785 (clone 30-F11)	BioLegend	Cat #: 103149; RRID:AB_2564590
rat anti-mouse CD4-APC-eFluor780 (clone RM4-5), eBioscience	Invitrogen	Cat #: 47-0042; RRID:AB_1272183
rat anti-CD8a-PeCy7 (clone 53-6.7) , eBioscience	Invitrogen	Cat #: 25-0081; RRID:AB_469584
hamster anti-mouse TCR gamma/delta PerCP-eFluor 710 (clone eBioGL3), eBioscience	Invitrogen	Cat #: 46-5711; RRID:AB_2016638

(*Continued on next page*)

Continued

REAGENT or RESOURCE	SOURCE	IDENTIFIER
rat anti-IL-17A-FITC (clone eBio17B7), eBioscience	Invitrogen	Cat #: 11-7177; RRID:AB_763581
rat anti-mouse GM-CSF-PE (clone MP1-22E9), eBioscience	Invitrogen	Cat #: 12-7331; RRID:AB_466203
rat anti-mouse CD25-Brilliant Violet 605 (clone PC61)	BioLegend	Cat #: 102036; RRID:AB_2563059
rat anti-mouse IFN-γ- Brilliant Violet 711 (clone XMG1.2)	BioLegend	Cat #: 505835; RRID:AB_11219588
rat anti-Ki67-eFluor450 (clone SolA15), eBioscience	Invitrogen	Cat #: 48-5698; RRID:AB_11149124
rat anti-Foxp3-APC (clone FJK-16s), eBioscience	Invitrogen	Cat #: 17-5773; RRID:AB_469457
monoclonal rabbit anti-histone 3 (clone D1H2)	Cell Signaling Technology	Cat #: 4499; RRID:AB_10544537
monoclonal mouse anti-β-actin (clone AC-74)	Sigma Aldrich	Cat #: A5316; RRID:AB_476743
monoclonal rabbit anti-PKM1 (clone D30G6)	Cell Signaling Technology	Cat #: 7067; RRID:AB_2715534
monoclonal rabbit anti-PKM2 (clone D78A4)	Cell Signaling Technology	Cat #: 4053; RRID:AB_1904096
polyclonal rabbit anti-alpha tubulin	Cell Signaling Technology	Cat #: 2144; RRID:AB_2210548
polyclonal rabbit anti-c-Myc	Cell Signaling Technology	Cat #: 9402; RRID:AB_2151827
polyclonal rabbit anti-phospho-p70 S6 Kinase (Thr389)	Cell Signaling Technology	Cat #: 9205; RRID:AB_330944
monoclonal rabbit anti-Hif-1α (clone D2U3T)	Cell Signaling Technology	Cat #: 14179; RRID:AB_2622225
polyclonal rabbit anti-phospho-PKM2 (Tyr105)	Cell Signaling Technology	Cat #: 3827; RRID:AB_1950369
polyclonal rabbit anti-phospho-PKM2 (Ser37)	Biorbyt	Cat #: orb336828
monoclonal rabbit anti-Stat5 (clone D206Y)	Cell Signaling Technology	Cat #: 94205; RRID:AB_2737403
monoclonal rabbit anti-phospho-Stat5 (Tyr694) (clone D47E7)	Cell Signaling Technology	Cat #: 4322; RRID:AB_10544692
Biological Samples		
Blood samples from healthy donors	School of Biochemistry and Immunology, TCD	N/A
Chemicals, Peptides, and Recombinant Proteins		
CD62L MicroBeads, mouse	Miltenyi Biotec	Cat #: 130-049-701
Mouse IL-12	Miltenyi Biotec	Cat #: 130-096-708
Recombinant Mouse IL-23 (carrier-free)	BioLegend	Cat #: 589002; RRID:AB_10663413
Recombinant Human TGF-β1	ImmunoTools	Cat #: 1134316
Recombinant Murine IL-1β	ImmunoTools	Cat #: 1234001
Recombinant Murine IL-6	ImmunoTools	Cat #: 1234006
TEPP-46	National Center for Advancing Translational Sciences (NIH; Bethesda, Maryland, USA)	CAS: 1221186-53-3
DASA-58	Cayman Chemical	Cat #: 13941; CAS: 1203494-49-8
DSS	Thermo Scientific	Cat #: 21655; CAS: 68528-80-3

(*Continued on next page*)

Continued

REAGENT or RESOURCE	SOURCE	IDENTIFIER
WesternBright ECL	Advansta	Cat #: K-12049-D50
Propidium Iodide	Invitrogen	Cat #: P1304MP; CAS: 25535-16-4
Pacific Blue™ Annexin V	BioLegend	Cat #: 640918
PMA	Sigma Aldrich	Cat #: P8139; CAS:16561-29-8
Ionomycin	Sigma Aldrich	Cat #: I0634; CAS: 56092-82-1
Brefeldin A	Sigma Aldrich	Cat #: B7651; CAS: 20350-15-6
Fixation Buffer	BioLegend	Cat #: 420801
Intracellular Staining Permeabilization Wash Buffer (10X)	BioLegend	Cat #: 421002
Seahorse XF Medium	Agilent	Cat #: 103575
Cell-Tak	Corning	Cat #: 354240
Olgomycin	Sigma Aldrich	Cat #: 495455; CAS: 1404-19-9
2-deoxy-d-glucose	Sigma Aldrich	Cat #: D3179; CAS: 154-17-6
FCCP	Sigma Aldrich	Cat #: C2759; CAS: 555-60-2
Antimycin A	Sigma Aldrich	Cat #: A8674; CAS: 1397-94-0
Rotenone	Sigma Aldrich	Cat #: R8875; CAS: 83-79-4
MOG_{35-55}	GenScript	Cat #: RP10245; CAS: 163913-87-9
Complete Freund Adjuvant	Chondrex	Cat #: 7001
Pertussis toxin	Kaketsuken	N/A
(2-Hydroxypropyl)-β-cyclodextrin	Sigma Aldrich	Cat #: H107; CAS: 128446-35-5
Protein Transport Inhibitor (BD GolgiStop)	BD Biosciences	Cat #: 554724
Purified Rat Anti-Mouse CD16/CD32 (Mouse BD Fc Block™)	BD Biosciences	Cat #: 553141; RRID:AB_394656
Critical Commercial Assays		
CD4+ T Cell Isolation Kit, mouse	Miltenyi Biotec	Cat #: 130-104-454
Naive CD4+ T Cell Isolation Kit, mouse	Miltenyi Biotec	Cat #: 130-104-453
Naive CD4+ T Cell Isolation Kit II, human	Miltenyi Biotec	Cat #: 130-094-131
Pan T Cell Isolation Kit II, mouse	Miltenyi Biotec	Cat #: 130-095-130
Seahorse XFe96 FluxPak	Agilent	Cat #: 102416–100
PARIS Kit	Invitrogen	Cat #: AM1921
PureLink RNA Mini Kit	Invitrogen	Cat #: 12183025
High-Capacity cDNA Reverse Transcription Kit	Applied Biosystems	Cat #: 4368814
PowerUp SYBR Green Master Mix	Applied Biosystems	Cat #: A25743
CellTrace Violet Cell Proliferation Kit	Invitrogen	Cat #: C34571
eBioscience Foxp3 / Transcription Factor Staining Buffer Set	Invitrogen	Cat #: 00-5523-00
LIVE/DEAD Fixable Aqua Dead Cell Stain Kit	Invitrogen	Cat #: L34965
Pierce™ BCA Protein Assay Kit	Thermo Scientific	Cat #: 23227
NEBNext Single Cell/Low Input RNA Library Prep Kit for Illumina	New England BioLabs	Cat #: E6420

(*Continued on next page*)

Continued

REAGENT or RESOURCE	SOURCE	IDENTIFIER
Deposited Data		
RNA sequencing data	This paper	GEO: GSE139378
Experimental Models: Organisms/Strains		
Mouse: C57BL/6JOlaHsd	Harlan UK	N/A
Oligonucleotides		
mouse *Tbp* FWD: CCGTGAATCTTGGCTGTAAAC mouse *Tbp* REV: TGTCCGTGGCTCTCTTATTC	Eurofins Genomics	N/A
mouse *Pkm1* FWD: TGTCTGGAGAAACAGCCAAG mouse *Pkm1* REV: CTCGCACAAGCTCTTCAAAC	Eurofins Genomics	N/A
mouse *Pkm2* FWD: TGTCTGGAGAAACAGCCAAG mouse *Pkm2* REV: CGAATAGCTGCAAGTGGTAGA	Eurofins Genomics	N/A
mouse *Il2* FWD: AGATGAACTTGGACCTCTGCG mouse *Il2* REV: AAAGTCCACCACAGTTGCTG	Eurofins Genomics	N/A
mouse *Tnfa* FWD: GCCTCTTCTCATTCCTGCTT mouse *Tnfa* REV: TGGGAACTTCTCATCCCTTTG	Eurofins Genomics	N/A
mouse *Foxp3* FWD: TTTCACCTATGCCACCCTTATC mouse *Foxp3* REV: GTAGGCGAACATGCGAGTAA	Eurofins Genomics	N/A
mouse *Hif1a* FWD: GGGTACAAGAAACCACCCAT mouse *Hif1a* REV: GAGGCTGTGTCGACTGAGAA	Eurofins Genomics	N/A
mouse *Myc* FWD: TTGAAGGCTGGATTTCCTTTGGGC mouse Myc REV: TCGTCGCAGATGAAATAGGGCTGT	Eurofins Genomics	N/A
mouse *Slc2a1* FWD: GATCACTGCAGTTCGGCTATAA mouse *Slc2a1* REV: GTAGCGGTGGTTCCATGTT	Eurofins Genomics	N/A
mouse *Gapdh* FWD: TGGTGAAGGTCGGTGTGAAC mouse *Gapdh* REV: TGAATTTGCCGTGAGTGGAG	Eurofins Genomics	N/A
mouse *Ldha* FWD: CGTCTCCCTGAAGTCTCTTAAC mouse *Ldha* REV: TTCAGCTTGATCACCTCGTAG	Eurofins Genomics	N/A
mouse *Hk* FWD: TCGCCTGCTTATTCACGGAG mouse *Hk* REV: CCATCCGGAGTTGACCTCAC	Eurofins Genomics	N/A
mouse *Pfkm* FWD: GTTTGGAAGCCTCTCCTCCTC mouse *Pfkm* FWD: AGAGGTCAACACGGCGATG	Eurofins Genomics	N/A
mouse *Il17a* FWD: CAAACATGAGTCCAGGGAGAG mouse *Il17a* REV: GCTGAGCTTTGAGGGATGAT	Eurofins Genomics	N/A
mouse *Il17f* FWD: TCCCACGTGAATTCCAGAAC mouse *Il17f* REV: GTTCATGGTGCTGTCTTCCT	Eurofins Genomics	N/A
mouse *Il21* FWD: CGCCTCCTGATTAGACTTCG mouse *Il21* REV: GCCCCTTTACATCTTGTGGA	Eurofins Genomics	N/A
mouse *Il22* FWD: TCATCGGGGAGAAACTGTTC mouse *Il22* REV: TTCCAGGGTGAAGTTGAGCA	Eurofins Genomics	N/A
mouse *Rora* FWD: GAACACCTTGCCCAGAACAT mouse *Rora* REV: AGCTGCCACATCACCTCTCT	Eurofins Genomics	N/A
mouse *Runx1* FWD: TACCTGGGATCCATCACCTC mouse *Runx1* REV: GACGGCAGAGTAGGGAACTG	Eurofins Genomics	N/A
mouse *Irf4* FWD: GCAGCTCACTTTGGATGACA mouse *Irf4* REV: CCAAACGTCACAGGACATTG	Eurofins Genomics	N/A
mouse *Rorc* FWD: TGCAAGACTCATCGACAAGGC mouse *Rorc* REV: AGCTTTTCCACATGTTGGCTG	Eurofins Genomics	N/A
mouse *Ahr* FWD: AGGTGCCTGCTGGATAATTC mouse *Ahr* REV: CCGTCCTTCCCTTTCTTGTT	Eurofins Genomics	N/A
mouse *Nzkbiz* FWD: GCAGGTAGAGCAGGAAGAAA mouse *Nzkbiz* REV: CCTTGGGCAACAGCAATATG	Eurofins Genomics	N/A

(*Continued on next page*)

Continued

REAGENT or RESOURCE	SOURCE	IDENTIFIER
mouse *Batf* FWD: CCAGAAGAGCCGACAGAGAC mouse *Batf* REV: GAGCTGCGTTCTGTTTCTCC	Eurofins Genomics	N/A
mouse *Ifng* FWD: CTCTTCTTGGATATCTGGAGGAAC mouse *Ifng* REV: GACTTCAAAGAGTCTGAGGTAGAA	Eurofins Genomics	N/A
mouse *Tbx21* FWD: CAACAACCCCTTTGCCAAAG mouse *Tbx21* REV: TCCCCCAAGCAGTTGACAGT	Eurofins Genomics	N/A
mouse *Eomes* FWD: ACCAATAACAAAGGTGCAAACAAC mouse *Eomes* REV: TGGTATTTGTGCAGAGACTGCAA	Eurofins Genomics	N/A
human *RPS13* FWD: CGAAAGCATCTTGAGAGGAAC human *RPS13* REV: TCGAGCCAAACGGTGAATC	Eurofins Genomics	N/A
human *PKM1* FWD: TCACTCCACAGACCTCATGG human *PKM1* REV: GAAGATGCCACGGTACAGGT	Eurofins Genomics	N/A
human *PKM2* FWD: ATCGTCCTCACCAAGTCTGG human *PKM2* REV: GAAGATGCCACGGTACAGGT	Eurofins Genomics	N/A
human *IL2* FWD: CCCAGGGACTTAATCAGCAATA human *IL2* REV: TGCTGTCTCATCAGCATATTCA	Eurofins Genomics	N/A
Software and Algorithms		
Image Lab (Version 5.0)	Bio-Rad	https://www.bio-rad.com/en-uk/product/image-lab-software?ID=KRE6P5E8Z
FlowJo (version 10.5.3)	FlowJO	https://www.flowjo.com/solutions/flowjo
Seahorse Wave Controller Software (version 2.4.2)	Agilent	https://www.agilent.com/en/products/cell-analysis/cell-analysis-software/instrument-software/wave-controller-2-4
Prism (version 8.2.0)	GraphPad	https://www.graphpad.com/scientific-software/prism/
SnakePipes (version 1.2.0)	Bhardwaj et al., 2019	N/A
DESeq2 R	Love et al., 2014	N/A
Ingenuity Pathway Analysis	Qiagen	https://www.qiagenbioinformatics.com/products/ingenuity-pathway-analysis/
Morpheus	Broad Institute, Cambridge, MA, (USA)	https://software.broadinstitute.org/morpheus/

LEAD CONTACT AND MATERIALS AVAILABILITY

This study did not generate new unique reagents. We are glad to share the commercially available reagents used in this study with reasonable compensation by requestor for their processing and shipping. Further information and requests for resources and reagents should be directed to and will be fulfilled by the Lead Contact, Stefano Angiari (angiaris@tcd.ie).

EXPERIMENTAL MODEL AND SUBJECT DETAILS

Mice

6-8 weeks old C57Bl/6J female mice (Harlan UK) were used to isolate murine T cells and for EAE experiments. Mice were bred and housed in the Comparative Medicine Unit (CMU) in Trinity Biomedical Sciences Institute (TBSI) (Trinity College Dublin, TCD, Ireland), and maintained under specific pathogen free conditions according to FELASA guidelines (Mähler Convenor et al., 2014). All the procedures involving experiments on animals have been approved by the Health Products Regulatory Authority (HPRA, Ireland), and were conducted according to Directive 2010/63/EU of the European Parliament and Council on the protection of animals used for scientific purposes. Before each experiment, mice were randomly assigned to control or treatment group. No sample-size estimation was performed before experimentation.

Human Samples

Human blood samples from healthy donors were collected and processed at the School of Biochemistry and Immunology in TBSI (TCD, Ireland). Blood samples have been obtained anonymously and written informed consent for the use of blood for research

purposes has been obtained from the donors. All the procedures involving experiments on human samples have been approved by the School of Biochemistry and Immunology Research Ethics Committee (TCD). Experiments were conducted according to the TCD guide on good research practice, which follows the guidelines detailed in the National Institutes of Health Belmont Report (1978) and the Helsinki Declaration (revised 2013).

METHOD DETAILS

Cell Isolation and Cultures

Murine $CD4^+$ T cells were obtained from total mouse splenocytes by magnetic cells sorting with the $CD4^+$ T Cell Isolation Kit, followed by incubation with CD62L microbeads and isolation of $CD4^+CD62L^+$ resting T cells, following manufacturer's instructions (all reagents from Miltenyi Biotech). In some experiments, naïve $CD4^+$ murine T cells were isolated from total splenocytes by magnetic cell sorting with the Naive $CD4^+$ T Cell Isolation Kit (Miltenyi Biotech). For human samples, peripheral blood mononuclear cells (PBMCs) were isolated from whole blood by density centrifugation in Lymphoprep (StemCell Technologies). Naïve $CD4^+$ T cells were then obtained from PBMCs by magnetic cell sorting with the Naïve $CD4^+$ T Cell Isolation Kit II, according to manufacturer's instructions (Miltenyi Biotech). Cells were stimulated *in vitro* with plate-bound anti-CD3 and anti-CD28 antibodies (1 μg/ml and 2 μg/ml, respectively) in RPMI 1640 containing L-glutamine (Gibco), supplemented with 10% heat-inactivated fetal bovine serum (Sigma-Aldrich), 55 μm 2-mercaptoethanol (Gibco) and 100 U/ml penicillin/streptomycin (Sigma-Aldrich). To generate murine T cell subsets, cells were activated in the presence of the following cytokines and antibodies: for Th1 cells, 20 ng/ml IL-12 and 5 μg/ml anti-mouse IL-4 antibody; for Th17 cells, 0.5 ng/ml TGF-β, 50 ng/ml IL-6, 10 ng/ml IL-23, 10 ng/ml IL-1β, 5 μg/ml anti-mouse IFN-γ antibody and 5 μg/ml anti-mouse IL-4 antibody; for Tregs, 5 ng/ml TGF-β. Antibodies were purchased from BD Biosciences, while cytokines were purchased from Miltenyi Biotech, Immunotools or BioLegend. For PKM2 tetramerisation experiments, TEPP-46 and DASA-58 (Cayman Chemical) were dissolved at a concentration of 100 mM in dimethyl sulfoxide (DMSO) and stored at -20°C until use. Cells were pre-incubated at 37°C for 15 min with TEPP-46 or DASA-58 25 μm, 50 μm or 100 μm or equal amounts of DMSO (control condition) before CD3/CD28 activation.

Nuclear Extraction, PKM2 Crosslinking, and Western Blotting

For standard western blot protocols, cultured cells were collected and lysed in 5× Laemmli Sample Buffer, followed by heating at 95°C for 5 min. For nuclear extraction experiments, nuclear and cytoplasmic fractions were isolated from cultured cells by cell fractionation using the PARIS^{T}kit (Invitrogen), following manufacturer's instructions. Protein concentration was measured using the Pierce BCA protein assay (Thermo Scientific) and normalised across samples prior to loading on SDS-PAGE gels for western blotting. For PKM2 crosslinking experiments, cells were collected, washed twice with phosphate buffered saline (PBS) pH 8.0 and incubated in PBS pH 8.0 + 1 μM disuccinimidyl suberate (DSS; Thermo Scientific) for 30 min at 37°C. Cells were then washed, lysed in 5× Laemmli Sample Buffer, and boiled for 5 min at 95 °C before loading. Protein samples were resolved on SDS-PAGE gels and transferred onto a polyvinylidene difluoride (PVDF) membrane via wet transfer. Membranes were probed with primary antibodies at a 1:1000 dilution and secondary HRP-conjugated antibodies at a 1:2000 dilution. Membranes were visualised using WesternBright ECL HRP substrate (Advansta) on a GelDoc system (Bio-Rad). Images were analysed with the Image Lab software (Bio-Rad). Histone H3 or β-actin were used as reference housekeeping genes.

Quantitative Real-Time PCR (qRT-PCR)

RNA was isolated using the Purelink RNA Mini kit (Invitrogen), according to manufacturer's instructions. RNA was converted to cDNA using the High Capacity cDNA Reverse Transcription Kit (Applied Biosystems), and gene expression was determined by qRT-PCR using the PowerUp SYBR Green Master on a 7500 Fast thermocycler (Applied Biosystems). For murine cells, gene expression was normalised to the reference housekeeping gene TATA-binding protein (*Tbp*), while for human cells gene expression was normalised to ribosomal protein S13 (*RPS13*). All primers were purchased from Eurofins Genomics.

Flow Cytometry

All flow cytometry analyses were performed after 3 days (72 hours; murine cells) or 4 days (96 hours; human cells) post-activation, apart from evaluation of early IL-2 production, which was analysed at 24 hours (murine cells) and 48 hours (human cells) post-activation. All antibodies for flow cytometry staining were used at 1:200 dilution. To determine TEPP-46 toxicity, cells were stained with propidium iodide (PI; Invitrogen) and Pacific Blue-conjugated annexin V (AV; BioLegend). Cells were then gated as live (PI^-AV^-), apoptotic (PI^-AV^+) or necrotic/dead cells (PI^+AV^+). For analysis of cell proliferation, cells were pre-stained with fluorescent CellTrace Violet (CTV; Invitrogen) before activation, according to manufacturer's instructions. Cell proliferation was evaluated as CTV dilution as previously described (Hawkins et al., 2007). To evaluate T cell activation, cells were collected, washed and stained with anti-mouse CD62L, CD44 and CD25 antibodies (murine cells) or anti-human CD71 antibody (human cells). For intracellular cytokine staining, cells were collected, washed and re-stimulated with 50 ng/ml phorbol 12-myristate 13-acetate (PMA) + 1 μg/ml ionomycin + 10 μg/ml brefeldin A (all from Sigma Aldrich). After 4 hours, cells were washed, fixed/permeabilised with fixation and permeabilisation buffers (BioLegend) and stained with anti-mouse IL-2, IFN-γ, IL-17A and/or TNF-α (mouse cells) or anti-human TNF-α or IL-2. For Treg detection, cells were first stained with anti-mouse CD25 (mouse cells) or anti-human CD127 and CD25 antibodies (human cells). Cells were then fixed/permeabilised with Foxp3/Transcription Factor Staining Buffer Set (Invitrogen) and incubated with anti-mouse

or anti-human Foxp3 antibodies. All samples were analysed on a FACS Canto II Cell analyser (BD Biosciences). Analysis of acquired data was performed with the FlowJo software (FlowJo LLC). Antibodies were purchased from BD Biosciences, Invitrogen or BioLegend.

RNA Sequencing and Transcriptomics Analysis

Total RNA was quantified using Qubit 2.0 (Thermo Fisher Scientific). Libraries were prepared using the NEBNext Single Cell/Low Input RNA Library Prep Kit for Illumina (New England BioLabs) and sequenced using the HiSeq 3000 (Illumina) by the Deep Sequencing Facility at the Max Planck Institute of Immunobiology and Epigenetics (Freiburg, Germany). The quality of raw and trimmed Fastq reads was checked using FastQC (Illumina). Trimming of raw data was performed using the Cutadapt tool. STAR aligner (Dobin et al., 2013) was used to create BAM files, followed by gene-level quantification using featureCounts (Liao et al., 2014). This contains the gene-level counts, on the filtered GTF files, which were used for differential expression analysis. Gene-level differential expression analysis was then performed in R (Lucent Technologies) using the DESeq2 R package (Love et al., 2014). Principal component analysis plots were generated using in-house Rscripts. Unbiased pathway analysis was performed using Ingenuity Pathway Analysis (Qiagen). Only genes with calculated differential expression changes of >±1-fold change in TEPP-46-treated versus Th0 control samples and adjusted p value<0.05 were considered for pathway analysis. To generate heat maps of specific gene sets, the software Morpheus was used (Broad Institute). Gene lists were obtained from the publically available Geneset Enrichment Analysis (GSEA) database (Broad Institute) and other publications listed, and fold change gene expression of these gene sets were quantified in TEPP-46-treated Th0 versus control Th0 RNAseq data. Only genes with differential expression changes of >±1-fold change in TEPP-46-treated versus control samples and adjusted p value<0.05 were included in heat maps, which display raw read count values. HIF1A gene list was obtained from GSEA set M12299 ''SEMENZA_HIF1_TARGETS''. MYC gene list was obtained from GSEA set M5928 ''HALLMARK_MYC_TARGETS_V2''. MTOR gene list was obtained from GSEA set ''M16563 BIOCARTA_MTOR_PATHWAY''; this heat map shows all statistically significant changed genes in this set. Glycolysis gene list was obtained from GSEA set M5937 ''HALLMARK_GLYCOLYSIS''. T cell activation gene list was obtained from Panther Pathways accession P00053. Treg signature gene list was obtained by a detailed analysis of multiple peer-reviewed publications and publicly available gene sets from GSEA.

Analysis of ECAR and OCR with the Seahorse XF Platform

To evaluate extracellular acidification rate (ECAR) and OCR, 150,000 cells (ECAR assay) or 200,000 cells (OCR assay) in XF medium (Agilent) were seeded in a 96-well XF Cell Culture Microplate (Agilent) pre-coated with Cell-Tak™ (Corning). Cells were left to adhere for one hours at 37°C in the absence of CO_2. ECAR was then measured on a Seahorse XF Analyser (Agilent) in basal conditions and upon the sequential addition of glucose (20 mM), oligomycin (1 μM), and 2-deoxyglucose (2-DG; 50 mM) (all from Sigma Aldrich), to determine the glycolytic rate and the glycolytic capacity of tested cells. OCR was measured in basal conditions and upon the sequential addition of oligomycin (1 μM), carbonyl cyanide-4-(trifluoromethoxy)phenylhydrazone (FCCP; 1 μM), and rotenone/antimycin A (both at 0.5 μM) (all from Sigma Aldrich), to determine maximum respiration and spare respiratory capacity of tested cells.

Induction and Assessment of Active EAE

EAE was induced in 6–8 weeks old C57BL/6 female mice by subcutaneous immunization with 150 μg $MOG_{35–55}$ peptide (GenScript) emulsified in complete Freund's adjuvant (CFA; Condrex) containing 4 mg/ml heat-killed *Mycobacterium tuberculosis*. Mice were injected intraperitoneally (i.p.) with 200 ng pertussis toxin (Kaketsuken) on day 0 and +2 post-immunisation. For TEPP-46 treatment, mice were injected i.p. every other day from day 0 to day +14 post-immunisation with 200-μl vehicle (PBS + 40% cyclodextrin; Sigma-Aldrich) or 50 mg/kg TEPP-46 dissolved in vehicle. Mice were daily weighed and disease score was daily evaluated blinded as previously described (Sutton et al., 2017). In some experiments, EAE mice were sacrificed 11 days post-immunisation and perfused with 20 ml PBS. The central nervous system (CNS; brain and spinal cord) was then removed. CNS was lysed in RPMI containing brefeldin A (5 μg/ml) using a tissue lyser (Qiagen). CNS tissue homogenates were then re-suspended in 8 ml 40% isotonic Percoll before centrifugation at 1600 rpm for 20 min. Myelin debris was carefully removed, and CNS mononuclear cells were then passed through a 70 μm filter, washed, re-suspended in RPMI and stimulated with PMA (10 ng/ml), ionomycin (1 μg/ml), monensin (BD Golgistop, 1:1000; BD Biosciences) and brefeldin A (2 μg/ml) for 2 hours at 37°C. Cells were washed and incubated with live/dead stain (LIVE/DEAD Fixable Aqua Dead Cell Stain Kit: Life Technologies) for 20 min, followed by 10-min incubation with Fcγ block (BD Biosciences). Cells were then stained for 20 min with anti-mouse CD45, CD4, CD8α, TCRδ and CD25. Cells were then washed, fixed and permeabilised with the Foxp3/Transcription Factor Staining buffer Kit, and stained with antibodies specific for IL-17A, GM-CSF, IFN-γ, Foxp3 and Ki67. Cells were finally acquired using an LSRFortessa flow cytometer (BD Biosciences). Analysis of acquired data was performed with the FlowJo software. Analysis of stained population was performed by gating on single, live, $CD45^+$ cells. All antibodies were used at 1:200 dilution.

Induction of Transfer EAE in C57BL/6 Mice

6–8 weeks old C57BL/6 female mice were immunised as above with $MOG_{35–55}$ in CFA (no pertussis toxin injections). After 7 days, lymph nodes and spleen were collected, a single cell suspension obtained, and $CD3^+$ T cells were isolated by magnetic cell sorting using the Pan T cell Isolation Kit II (Miltenyi Biotech). $CD3^+$ cells were incubated with DMSO (control cells) or TEPP-46 100 μM for 4 hours at 37°C, washed twice and incubated in complete fresh medium with $CD3^-$ splenocytes in the presence of MOG_{35}–55

100 μg/ml + IL-1β 10 ng/ml and IL-23 10 ng/ml. After 3 days of restimulation, cells were collected, washed, and injected in equal numbers in recipient naïve C57BL/6 mice (15 million of total cells/mouse). EAE development was evaluated as described above.

QUANTIFICATION AND STATISTICAL ANALYSIS

Statistical analyses were performed using Prism 8 (GraphPad). Data were analysed by two-tailed Student's t-test or one-way ANOVA followed by Dunnett's post-hoc test for multiple comparisons. p values < 0.05 were considered statistically significant. The number of replicates (n), the number of independent experiments performed, and the p values for each experiment are reported in the corresponding figure legends. For both *in vivo* and *in vitro* experiments, no initial exclusion criteria were used and no animals or replicates were excluded from the study.

DATA AND CODE AVAILABILITY

The RNA sequencing data generated in this study have been deposited on the Gene Expression Omnibus (GEO) repository (accession number: GEO: GSE139378).

Cell Metabolism, Volume *31*

Supplemental Information

Pharmacological Activation of Pyruvate Kinase M2 Inhibits $CD4^+$ T Cell Pathogenicity and Suppresses Autoimmunity

Stefano Angiari, Marah C. Runtsch, Caroline E. Sutton, Eva M. Palsson-McDermott, Beth Kelly, Nisha Rana, Harry Kane, Gina Papadopoulou, Erika L. Pearce, Kingston H.G. Mills, and Luke A.J. O'Neill

SUPPLEMENTARY FIGURE TITLES AND LEGENDS

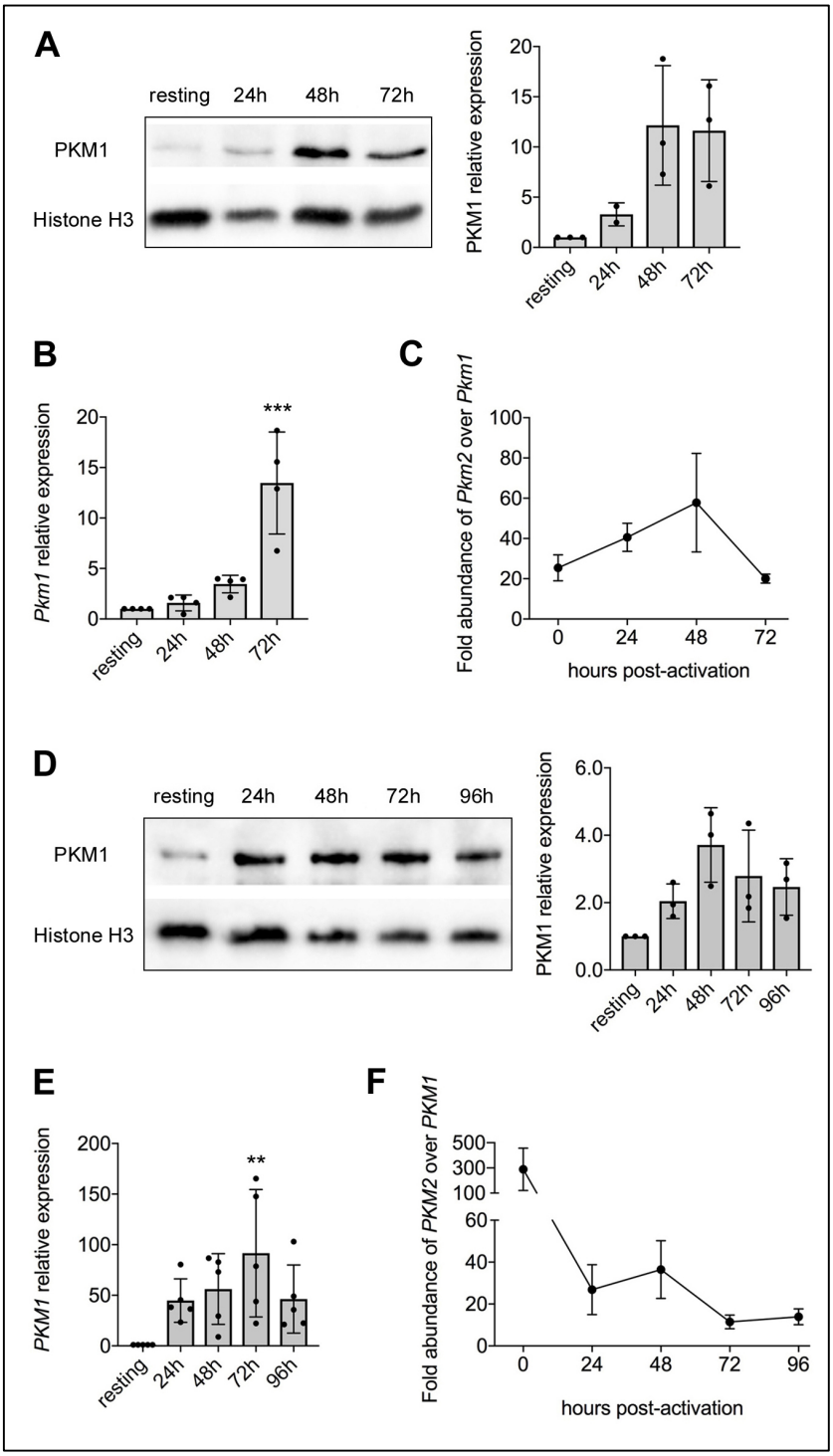

Figure S1. PKM1 expression in resting and activated murine and human CD4$^+$ T cells. Related to Figure 1 and 7. (**A-C**) Murine CD4$^+$CD62$^+$ T cells were stimulated *in vitro* for 3 days with CD3/CD28 antibodies and collected at different time points of activation. (**A**) Left: western blot showing upregulation of PKM1 protein in murine CD4$^+$ T cells following activation. Right: quantification of PKM1 expression by densitometry analysis (n=3 from two independent

experiments). (**B**) Quantification of *Pkm1* mRNA expression in resting versus activated murine $CD4^+$ T cells by qRT-PCR (n=4 from three independent experiments). ***P<0.001 compared to resting condition, by one-way Anova with Dunnett's post-hoc test. (**C**) Fold abundance of *Pkm2* over *Pkm1* mRNA in resting and activated murine $CD4^+$ T cells (n=4-6 from three-four independent experiments). (**D-F**) Human naïve $CD4^+$ T cells were stimulated *in vitro* for 4 days with anti-CD3/CD28 antibodies and collected at different time points of activation. (**E**) Left: western blot showing upregulation of PKM1 protein in human $CD4^+$ T cells following activation. Right: quantification of PKM1 expression by densitometry analysis (n=3 from three independent experiments). (**F**) Quantification of *Pkm1* mRNA expression in human $CD4^+$ T cells by qRT-PCR (n=5 from three independent experiments). **P<0.01 compared to resting condition, by one-way Anova with Dunnett's post-hoc test. (**C**) Fold abundance of *PKM2* versus *PKM1* expression levels in resting and activated human $CD4^+$ T cells (n=5 from three independent experiments). For all panels, data are the mean ± SD.

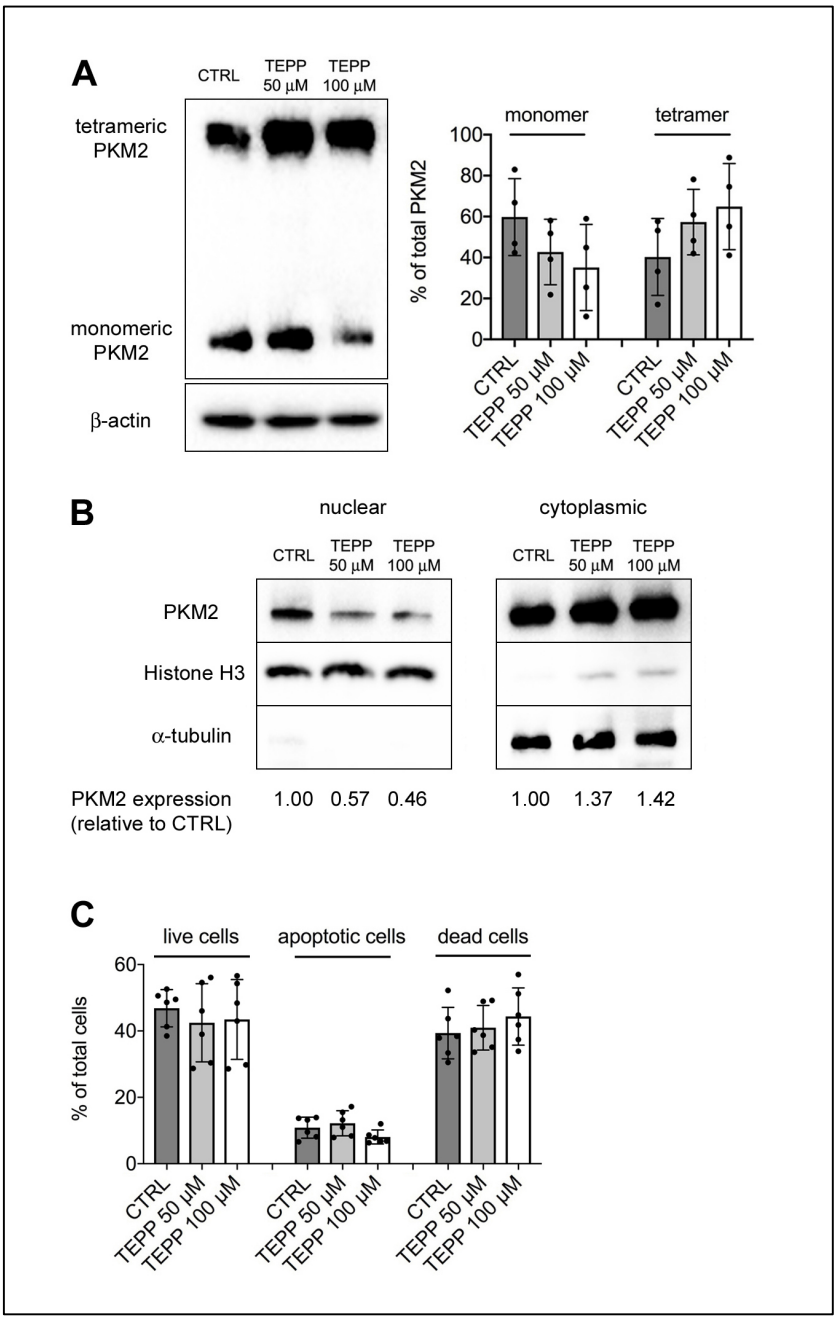

Figure S2. Effect of TEPP-46 on PKM2 tetramerisation, PKM2 nuclear translocation and T cell viability. Related to Figure 2. (**A**) Cells were collected after 3 days of stimulation, crosslinked with DSS and analysed for PKM2 expression. Left: Representative western blot showing induction of PKM2 tetrameric isoform by TEPP-46. Right: quantification of relative tetrameric and monomeric isoform expression over total PKM2 by densitometry analysis (n=4 from three independent experiments). (**B**) Cells were collected after 2 days of stimulation and PKM2 expression in nucleus and cytoplasm was analysed by western blot after cell fractionation. One representative experiment out of three showing a dose-dependent reduction of nuclear PKM2 expression in cells treated with TEPP-46 is displayed. (**C**) Murine $CD4^+$ T cells were collected after

3 days of activation in the presence of TEPP-46. Cells were stained with PI and Annexin V (AV) to determine live (PI^-AV^-), apoptotic (PI^-AV^+) or necrotic/dead cells (PI^+AV^+) (n=6 from three independent experiments). For all panels, data are the mean ± SD.

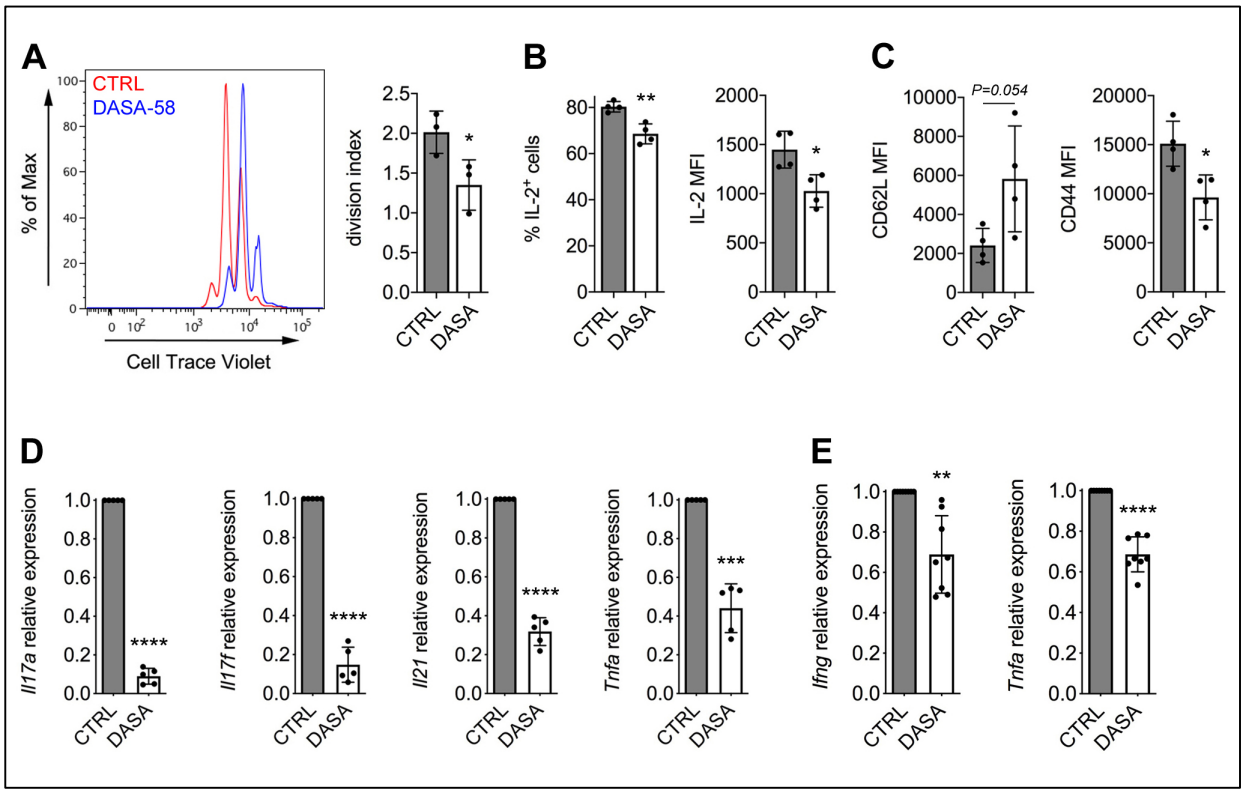

Figure S3. Effect of DASA-58 on CD4$^+$ T cell activation and generation of Th17 and Th1 cells *in vitro*. Related to Figure 2, Figure 4 and Figure 5. (**A-C**) Murine CD4$^+$CD62$^+$ T cells were activated *in vitro* with CD3/CD28 antibodies in the presence of DMSO (CTRL condition) or DASA-58 25 µM. (**A**) Cells were collected after 3 days of stimulation. Left: representative flow cytometry plot displaying T cell proliferation assessed as CellTrace^{TM} Violet dilution. Right: quantification of division index by FlowJo software (n=3 from two independent experiments). (**B**) Percentage of IL-2-producing cells and IL-2 MFI in CTRL versus DASA-58-treated cells 24 hours upon activation (n=4 from two independent experiments). (**C**) MFI of surface CD62L and CD44 expression, evaluated by flow cytometry. (n=4 from two independent experiments). (**D**) Murine CD4$^+$CD62$^+$ T cells were activated *in vitro* under Th17-polarising conditions in the presence of DMSO (CTRL condition) or DASA-58 100 µM. Expression of *Il17a*, *Il17f*, *Il21* and *Tnfa* mRNA in CTRL and DASA-treated Th17 cells was quantified by qRT-PCR (n=5 from two independent experiments). (**E**) Murine CD4$^+$CD62$^+$ T cells were activated *in vitro* under Th1-polarising conditions in the presence of DMSO (CTRL condition) or DASA-58 25 µM. Expression of *Ifng* and *Tnfa* mRNA in CTRL and DASA-treated Th1 cells was quantified by qRT-PCR (n=8 from three independent experiments). For all panels, data are the mean ± SD. *P<0.05, ** P<0.01, ***P<0.001 or ****P<0.0001 compared to CTRL condition, by unpaired (**A-C**) or paired (**D-E**) Student's t test.

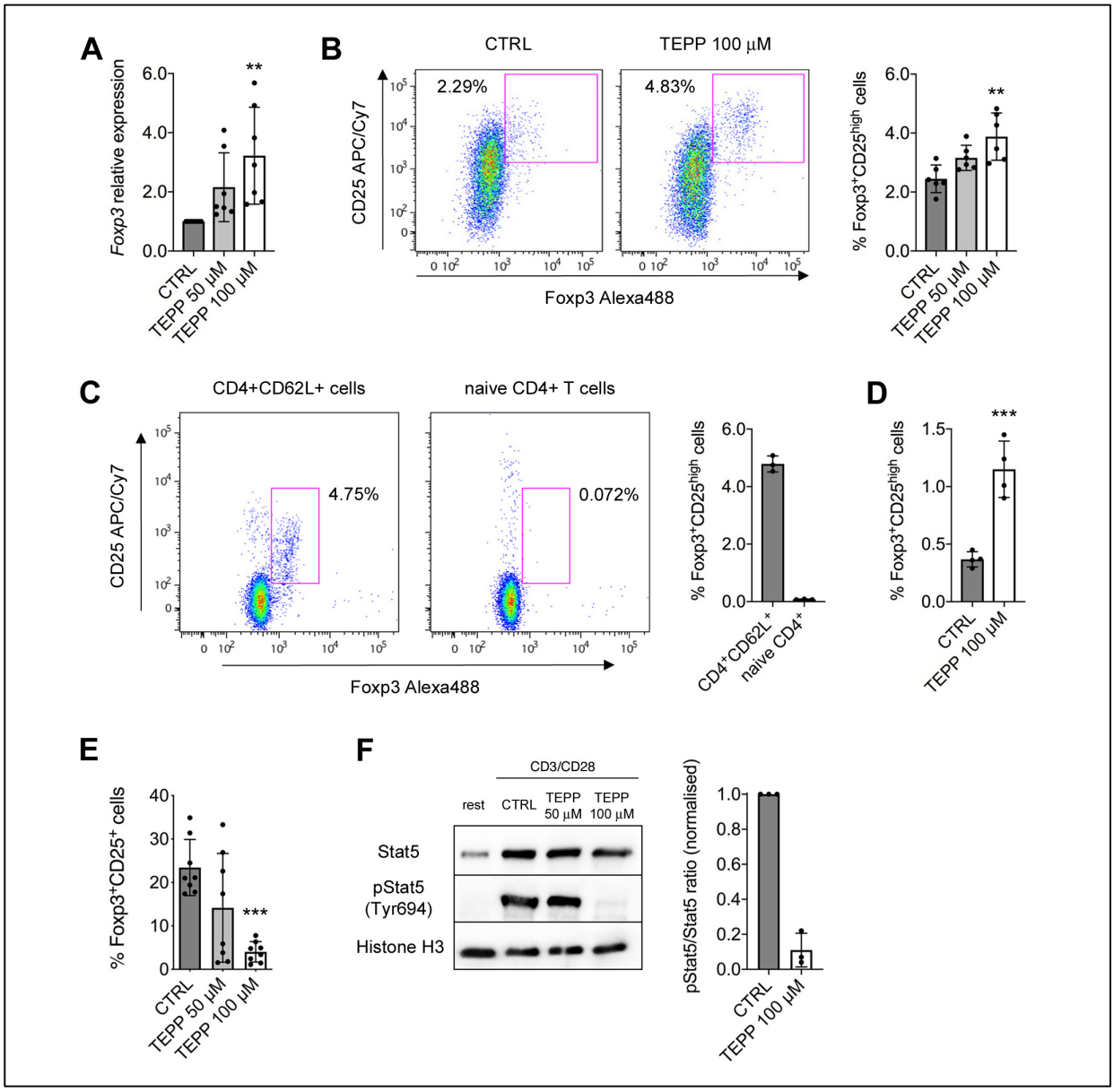

Figure S4. Induction of Foxp3$^+$CD25$^+$ T cells by TEPP-46 and effect of TEPP-46 on TGF-β-induced Tregs. Related to Figure 2. (**A**) Quantification of *Foxp3* mRNA levels by qRT-PCR in murine CD4$^+$ T cells activated in the presence of DMSO (CTRL condition) or TEPP-46 (n=7 from six independent experiments). (**B**) Left: representative plot showing induction of Foxp3$^+$CD25$^+$ T cells by TEPP-46 treatment. Right: quantification of the percentage of Foxp3$^+$CD25$^+$ T cells in CTRL and TEPP-46-treated cells (n=6 from four independent experiments). (**C**) Left: representative flow cytometry plots showing Foxp3$^+$CD25$^+$ T cells in freshly-isolated CD4$^+$CD62L$^+$ resting T cells and naïve CD4$^+$ T cells. Right: quantification of Foxp3$^+$CD25$^+$ T cell percentage in the two populations (n=3). (**D**) Naïve CD4$^+$ T cells were activated with CD3/CD28 antibodies in the presence of TEPP-46. The percentage of Foxp3$^+$CD25$^+$ T cells was evaluated after 3 days of stimulation. (n=4 from 2 independent experiments). (**E**) Murine CD4$^+$CD62$^+$ T cells were activated

in vitro with CD3/CD28 antibodies under Treg-polarising conditions, in the presence of TEPP-46. The percentage of $Foxp3^{+}CD25^{+}$ T cells in CTRL and TEPP-46-treated cells was quantified by flow cytometry (n=8 from four independent experiments). **(F)** Analysis of Stat5 phosphorylation in TGF-β-induced Tregs. Left: western blot showing block of Stat5 phosphorylation by TEPP-46. Right: quantification of phospho-Stat5/Stat5 ratio by densitometry analysis (n=3 from three independent experiments). In all panels, data are the mean the mean ± SD. $^{**}P<0.01$ or $^{***}P<0.001$, compared to CTRL condition, by one-way Anova with Dunnett's post-hoc test (**A, B** and **E**) or unpaired Student's t test (**D**).

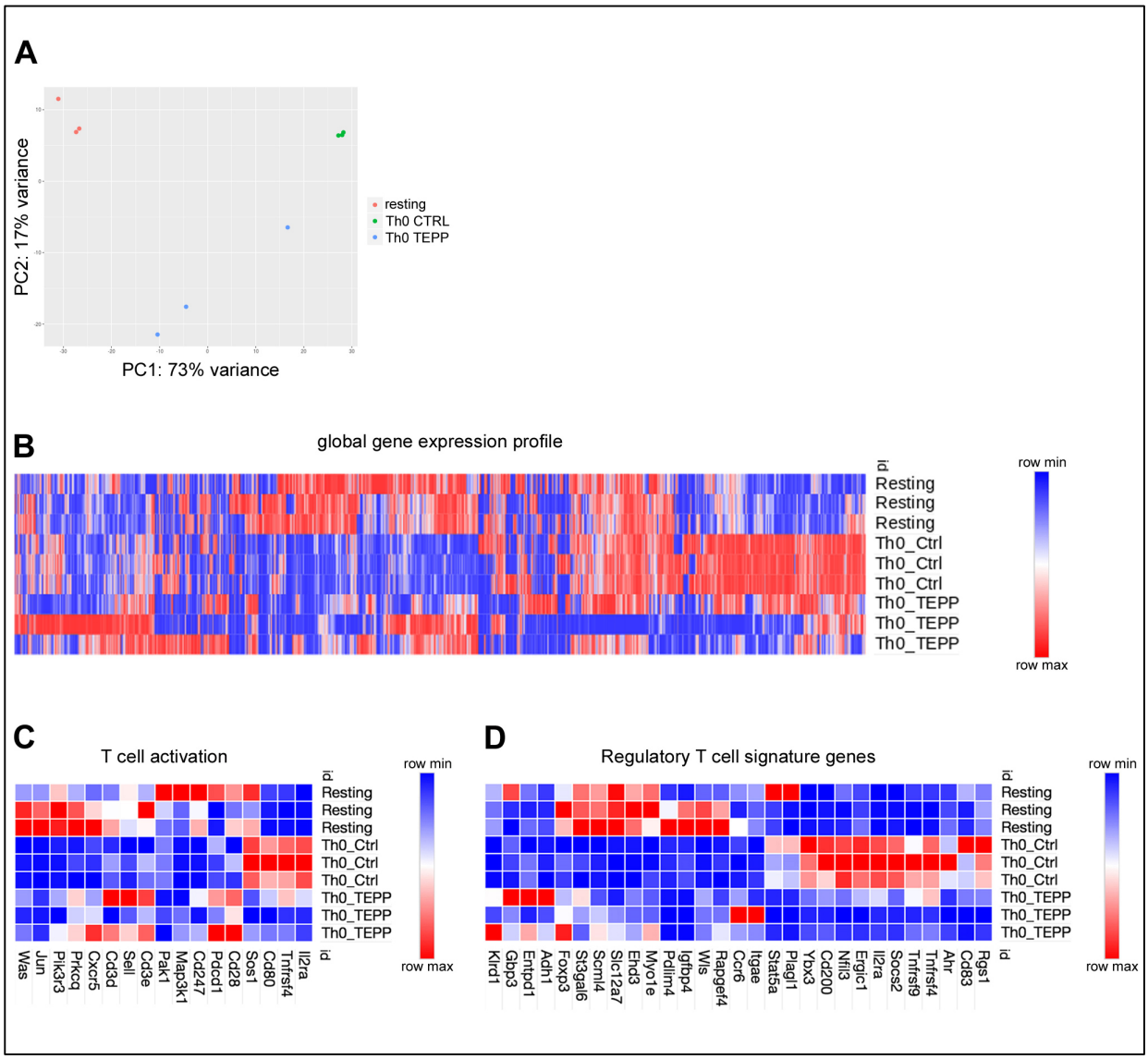

Figure S5. Global expression profile of resting CD4$^+$ T cells and CD4$^+$ T cells activated in the presence of DMSO (Th0 Ctrl) or TEPP-46 100 µM (Th0 TEPP). Related to Figure 2 and Figure 3. (**A**) Plot showing Principal Component analysis of global gene expression in the three T cell populations. (**B**) Heat map showing an overview of global gene expression in resting and Th0 Ctrl or Th0 TEPP-46 cells. (C) Heat map showing expression of genes related to T cells activation in the three populations. (D) Heat map showing expression of regulatory T cell signature genes in the three populations.

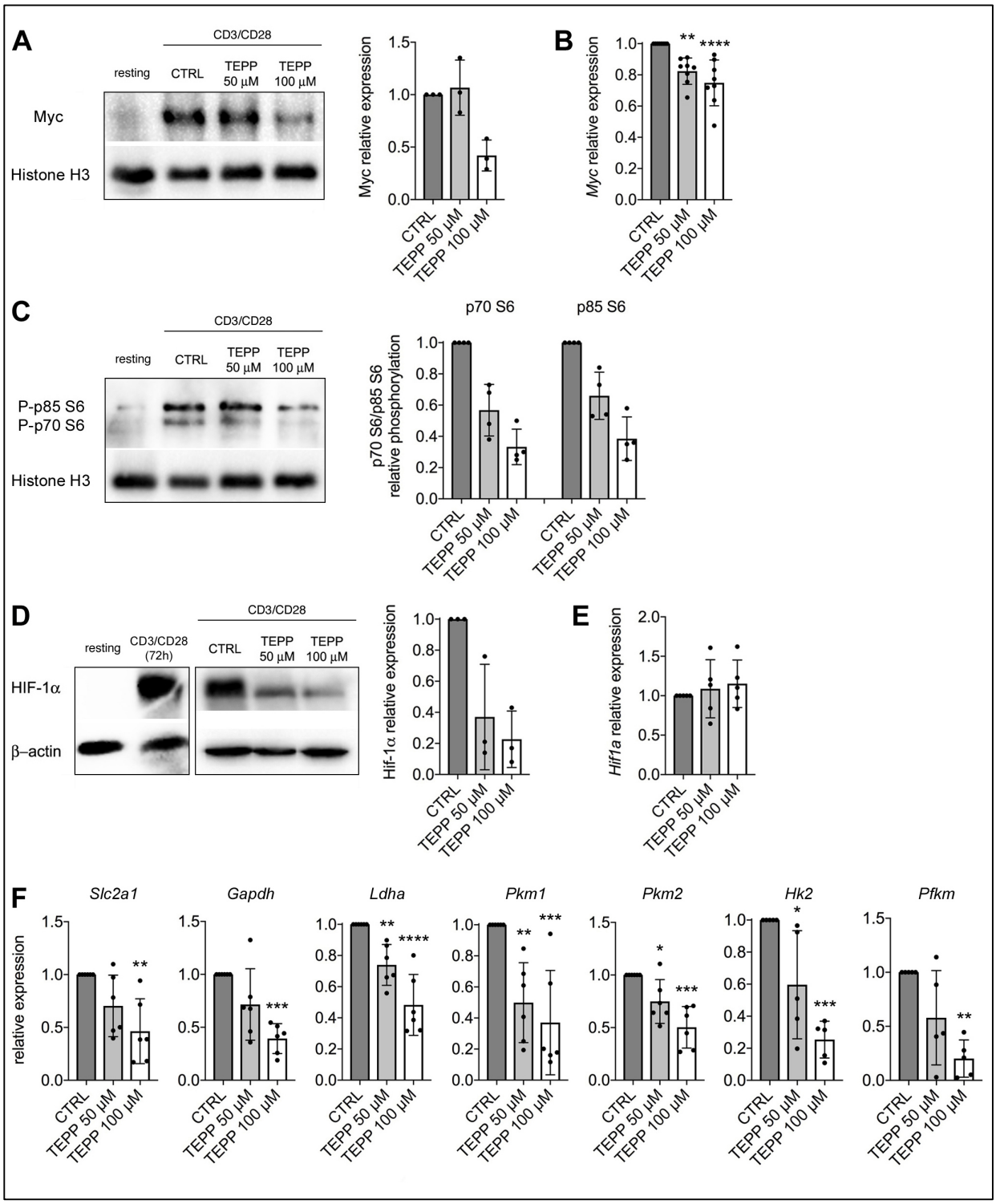

Figure S6. Effect of TEPP-46 on Myc and Hif-1α expression, mTORC1 activity and expression of glycolytic genes in activated T cells. Related to Figure 3. (**A** and **B**) Murine $CD4^+$ T cells were collected after 24 hours of *in vitro* activation with CD3/CD28 antibodies in the presence of DMSO (CTRL condition) or TEPP-46. (**A**) Left: western blot image showing reduction of Myc expression by TEPP-46 treatment. Right: quantification of relative Myc expression in

CTRL and TEPP-46-treated cells by densitometry analysis (n=3 from two independent experiments). (**B**) Quantification of *Myc* mRNA levels in CTRL and TEPP-46-treated cells by qRT-PCR (n=8 from 5 independent experiments). (**C**) Left: image from one representative experiment showing reduction of p70 S6 and p85 S6 phosphorylation by TEPP-46. Right: quantification of relative P-p70 S6 and P-p85 S6 band intensity by densitometry analysis (n=4 from two independent experiments). (**D-F**) Murine $CD4^+$ T cells were collected after 3 days of *in vitro* activation in the presence of DMSO or TEPP-46. (**D**) Left: western blot image showing Hif-1α downregulation in TEPP-46-treated cells, compared to CTRL cells. Right: quantification of relative Hif-1α expression by densitometry analysis (n=3 from two independent experiments). (**E**) *Hif1a* mRNA expression in CTRL and TEPP-46-treated cells quantified by qRT-PCR (n=5 from five independent experiments). (**F**) Expression of glycolytic genes in CTRL and TEPP-46-treated T cells by qRT-PCR (n=5-6 from 5 independent experiments). For all panels, data are the mean ± SD. **P*<0.05, ***P*<0.01, ****P*<0.001 or *****P*<0.0001, compared to CTRL condition, by one-way Anova with Dunnett's post-hoc test.

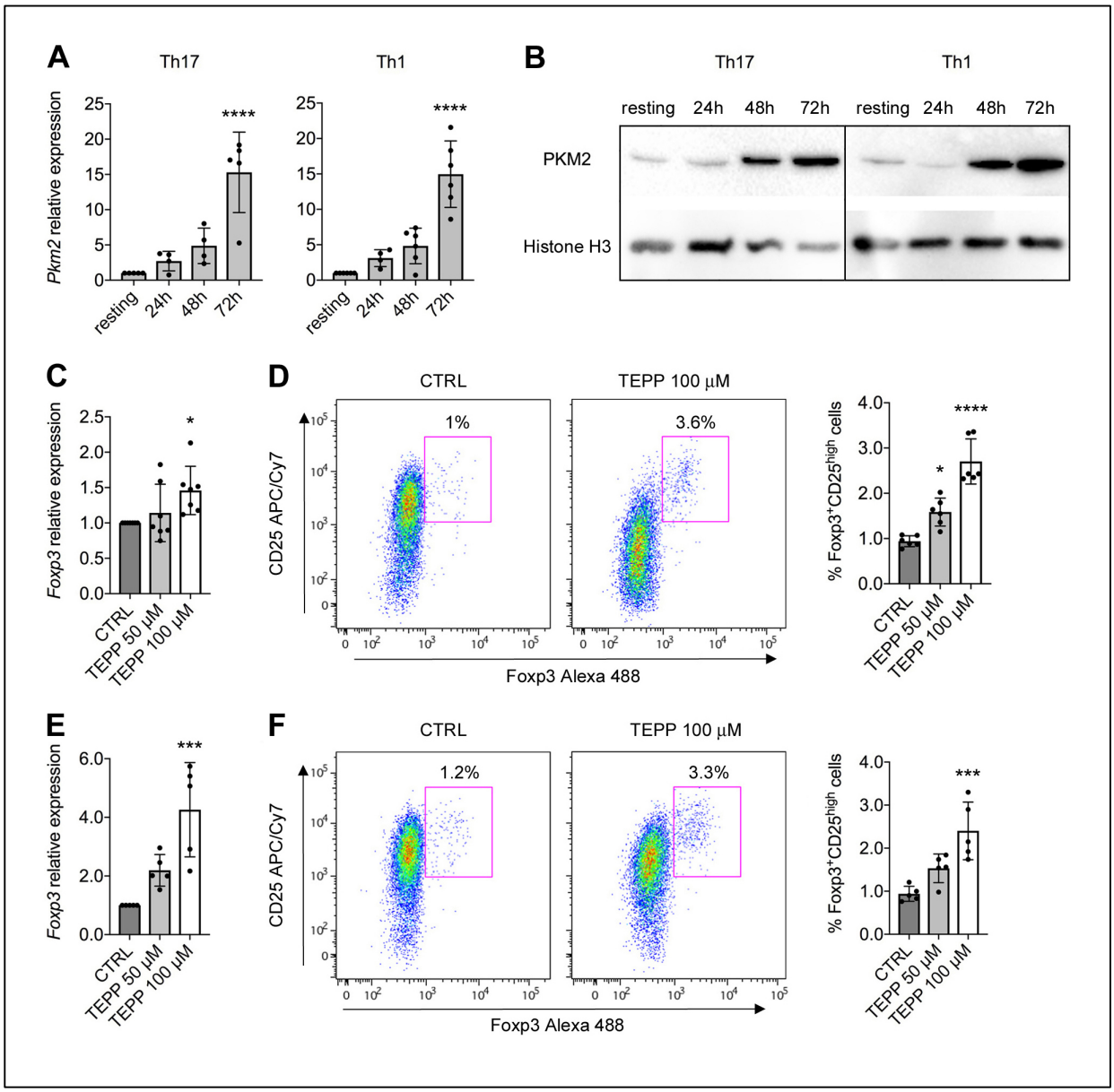

Figure S7. Expression of PKM2 in murine Th17 and Th17 cells and induction of Tregs under Th17 and Th17 polarising-conditions *in vitro*. Related to Figure 4 and 5. Murine $CD4^+CD62^+$ T cells were activated *in vitro* for 3 days with CD3/CD28 antibodies under Th17- or Th1-polarising conditions. (**A**) Quantification of *Pkm2* mRNA expression levels in resting $CD4^+CD62L^+$ T cells versus Th17 and Th1 cells at different time points of activation by qRT-PCR (n=4-6 from four independent experiments). (**B**) Western blot showing upregulation of PKM2 protein in Th17 and Th1 cells following activation. A representative experiment out of two is shown. (**C**) *Foxp3* gene expression in CTRL versus TEPP-46-treated Th17 cells (n=7 from four independent experiments). (**D**) Left: representative plot showing induction of $Foxp3^+CD25^+$ T cells under Th17-polarising conditions by TEPP-46. Right: quantification of the percentage of $Foxp3^+CD25^+$ T cells in CTRL and TEPP-46-treated cell populations (n=6 from two independent experiments). (**E**) *Foxp3*

expression in CTRL versus TEPP-46-treated Th1 cells (n=5 from three independent experiments). (**F**) Left: representative plot showing induction of $Foxp3^{+}CD25^{+}$ T cells by TEPP-46 under Th1-polarising conditions. Right: quantification of the percentage of $Foxp3^{+}CD25^{+}$ T cells in CTRL and TEPP-46-treated cell populations (n=5 from two independent experiments). For all panels, data are the mean ± SD. **P*<0.05, ****P*<0.001 or *****P*<0.0001, compared to CTRL condition, by one-way Anova with Dunnett's post-hoc test.